การสังเคราะห์แก๊สไอโซบิวทีนโดยตรงจากปฏิกิริยาคาร์บอนมอนอกไซด์ไฮโดรจิเนชันโดยใช้ตัวเร่งปฏิกิริยาเซอร์โคเนียมไดออกไซด์

(Direct Synthesis of Isobutene from CO Hydrogenation with ZrO_2 Catalysts)
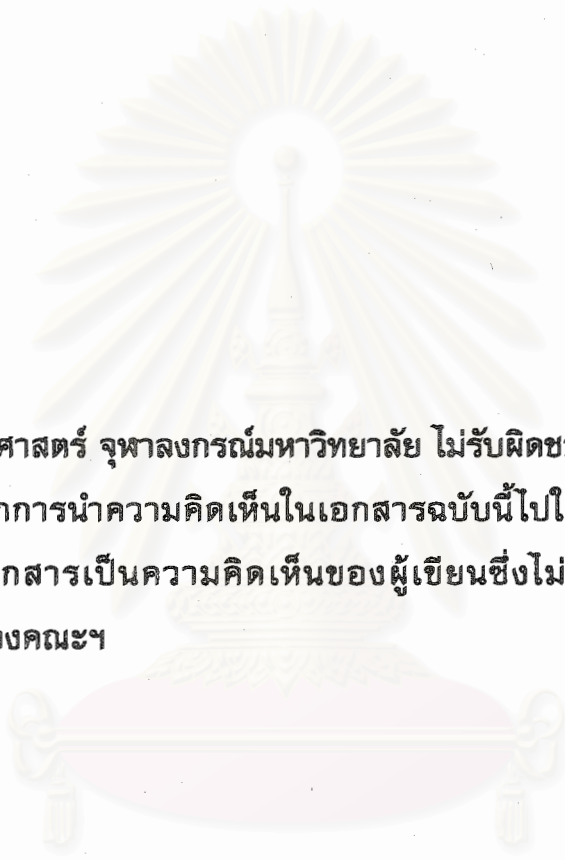
โดย

สุทธิชัย อัสสะบำรุงรัตน์

บรรเจิด จงสมจิตร

คณะวิศวกรรมศาสตร์

จุฬาลงกรณ์มหาวิทยาลัย

กรุงเทพฯ

กันยายน 2550

คณะวิศวกรรมศาสตร์ จุฬาลงกรณ์มหาวิทยาลัย ไม่รับผิดชอบต่อผลเสียใดๆ
อันอาจเกิดจากการนำความคิดเห็นในเอกสารฉบับนี้ไปใช้ ความคิดเห็น
ที่ปรากฏในเอกสารเป็นความคิดเห็นของผู้เขียนซึ่งไม่จำเป็นต้องเป็น
ความคิดเห็นของคณะฯ

การสังเคราะห์แก๊สไอโซบิวทีนโดยตรงจากปฏิกิริยาคาร์บอนมอนอกไซด์ไฮโดรจิเนชันโดยใช้ตัวเร่งปฏิกิริยาเซอร์โคเนียมไดออกไซด์

(Direct Synthesis of Isobutene from CO Hydrogenation with ZrO_2 Catalysts)

โดย

สุทธิชัย อัสสะบำรุงรัตน์ D.I.C., Ph.D.(London)

บรรเจิด จงสมจิตร Ph.D.(USA)

คณะวิศวกรรมศาสตร์

จุฬาลงกรณ์มหาวิทยาลัย

กรุงเทพฯ

กันยายน 2550

กิตติกรรมประกาศ

ii

บทคัดย่อ

โครงการวิจัยนี้ได้ศึกษาถึงพฤติกรรมในการเร่งปฏิกิริยาของตัวเร่งปฏิกิริยาเซอร์โคเนีย ที่มี
สมบัติแดกต่างกันในการสังเคราะห์ไอโซบิวทีน การศึกษาคุณลักษณะของตัวเร่งปฏิกิริยาเหล่านี้ทำ
โดยการใช้วิธีการวัดพื้นที่ผิว การกระเจิงรังสีเอ็กซ์ การคายซับของแอมโมเนียและ
คาร์บอนไดออกไซด์แบบโปรแกรมอุณหภูมิ และการส่องผ่านด้วยกล้องจุลทรรศน์อิเล็กตรอน/การวัด
การกระจายตัวของโลหะ งานวิจัยในส่วนแรกนั้นได้ศึกษาถึงผลของการใช้ตัวเร่งปฏิกิริยาเซอร์
โคเนียที่มีขนาดในระดับไมครอนและนาโนที่ต่างกันโดยเปรียบเทียบกับตัวเร่งปฏิกิริยาซีเรีย โดย
จากการศึกษาพบว่าตัวเร่งปฏิกิริยาที่มีขนาดในระดับนาโนจะให้ความว่องไวและค่าการเลือกเกิดของ
ไอโซบิวทีนที่มากกว่าตัวเร่งปฏิกิริยาที่มีขนาดในระดับไมครอน นอกจากนี้ยังพบว่าซีเรียจะให้ความ
ว่องไวที่มากกว่าเซอร์โคเนียแต่มีค่าการเลือกเกิดของไอโซบิวทีนที่ต่ำกว่า จากการศึกษาทำให้
อธิบายได้ว่าสมบัติความเป็นกรด-เบสและอัตราส่วนเฟสของเซอร์โคเนียสามารถส่งผลกระทบต่อ
พฤติกรรมในการเร่งปฏิกิริยาได้

งานวิจัยในส่วนที่สองได้ทำการศึกษาผลของอัตราการเพิ่มอุณหภูมิในการเผาตัวเร่งปฏิกิริยา
เซอร์โคเนียต่อพฤติกรรมการเร่งปฏิกิริยาของเซอร์โคเนียในการสังเคราะห์ไอโซบิวทีน โดยพบว่า
อัตราการให้ความร้อนที่สูงกว่าจะได้เฟสเตตระโกนอลเพิ่มขึ้น เมื่อพิจารณาถึงความว่องไวจะพบว่า
ค่าความเป็นกรดของเซอร์โคเนียจะไม่ส่งผลต่อความว่องไวในขณะที่ค่าความเป็นเบสจะมีผลต่อ
ความว่องไวและขึ้นกับสัดส่วนของเฟสเตตระโกนอลที่เพิ่มขึ้นและยังส่งผลต่อค่าการเลือกเกิดของไอ
โซบิวทีนอีกด้วย นอกจากนี้ยังพบว่าปริมาณของ Zr^{3+} ที่ผิวของเซอร์โคเนียที่วัดได้โดยใช้เครื่องมือ
อิเล็กตรอนสปินเรโซแนนซ์จะมีการเปลี่ยนแปลงเมื่อใช้อัตราการเพิ่มอุณหภูมิในการเผาเซอร์โคเนีย
ที่แตกต่างกัน ชี้ให้เห็นว่าทั้งปริมาณของเฟสเตตระโกนอลและ Zr^{3+} นั้น เป็นปัจจัยสำคัญที่ทำให้ค่า
การเลือกเกิดของไอโซบิวทีนต่างกันในปฏิกิริยาการสังเคราะห์ไอโซบิวทีน

Abstract

The focus of this research was to investigate the catalytic performances of various zirconia catalysts on isosynthesis. The characteristics of the catalysts were determined by means of various techniques including BET surface area, XRD, NH_3- and CO_2-TPD, TEM and SEM/EDX. In the first portion, different micron- and nanoscale zirconia catalysts were employed for the isosynthesis and compared with those of ceria. It was found that the nanoscale catalysts showed higher activity and selectivity of isobutene in hydrocarbons than the micronscale ones. Based on the nanoscale catalysts, ceria exhibited the highest activity among other zirconia catalysts, but lower selectivity for isobutene. In fact, the acid-base properties and phase composition of zirconia apparently influenced the catalytic performance.

In the second portion, effect of temperature ramp during calcination of zirconia on characteristics of nanoscale zirconia catalysts and their catalytic performance for isosynthesis was investigated. It was found that increased temperature ramp rate of calcination resulted in higher composition of tetragonal phase. Considering the catalytic activity, the acid sites did not affect activity, but the basic sites did which depended on the fraction of tetragonal phase in zirconia which was related to selectivity of isobutene. In particular, the intensity of Zr^{3+} on the surface obtained from the electron spin resonance spectroscopy (ESR) varied with the change in the heating rate of calcination. This indicated that the composition of tetragonal phase and Zr^{3+} were the key factors that can affect the selectivity of isobutene during isosynthesis.

CONTENTS

LIST OF TABLES

LIST OF FIGURES

CHAPTER I

INTRODUCTION

Isobutene, which is an extracted gas from C_4 stream of petroleum process, has been mainly used for producing oxygenated products such as ethyl *tert*-butyl ether (ETBE), methyl *tert*-butyl ether (MTBE) formed from the reactions of isobutene with ethanol and methanol, respectively. Demand of octane enhancers (such as ETBE and MTBE) is increasing with the increased fuel consumption every year. Because the presence of limit of isobutene sources which are mainly produced from petroleum, it is necessary to find out an alternative source for the production of isobutene. One of promising sources is isobutene synthesis from renewable resource such as biomass as shown in Figure 1.1. Firstly, biomass is fermented to produce methane (CH_4) and carbon dioxide (CO_2). Both of these products are used for synthesizing the synthesis gas, which consists of carbon monoxide (CO) and hydrogen (H_2), as shown by the following catalytic reaction

$$CH_4 + CO_2 \rightarrow 2CO + 2H_2$$

After that, synthesis gas is used for the next catalytic reaction forming isobutene as shown by the following the reaction:

$$4CO + 4H_2 \rightarrow i - C_4H_8$$
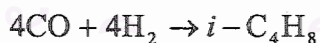
Advantages of this process are, firstly, the chosen resource of isobutene production is renewable. It is more attractive than the conventional petroleum sources which are about to shortage in the near future. Secondly, carbon dioxide from by product of fermentation process is consumed to produce synthesis gas, thus reducing the CO_2 emission to the atmosphere. CO_2 is considered as a major component causing the green house effect. Finally, ratio of carbon monoxide to hydrogen from the production of synthesis gas is 1:1 which is suitable for the reaction of isobutene synthesis.

1

Furthermore, the catalytic reaction that converts synthesis gas to branched chain hydrocarbons, especially isobutane and isobutene, is so-called isosynthesis. Early research (Pichler *et al.*, 1949) showed that oxide catalysts, such as thorium dioxide (ThO_2) and zirconium dioxide (ZrO_2), were usually used in this reaction. In addition, ThO_2 and ZrO_2 were the two most active catalysts but the recent research has focused on zirconia catalysts, because of their non-radioactivity and high selectivity to isobutene. Moreover, another oxide catalyst such as cerium dioxide (CeO_2) was also selective catalyst for the formation of branched chain compounds, i.e., isobutene in C_4 hydrocarbons from CO and H_2 (Maruya *et al.*, 1992).
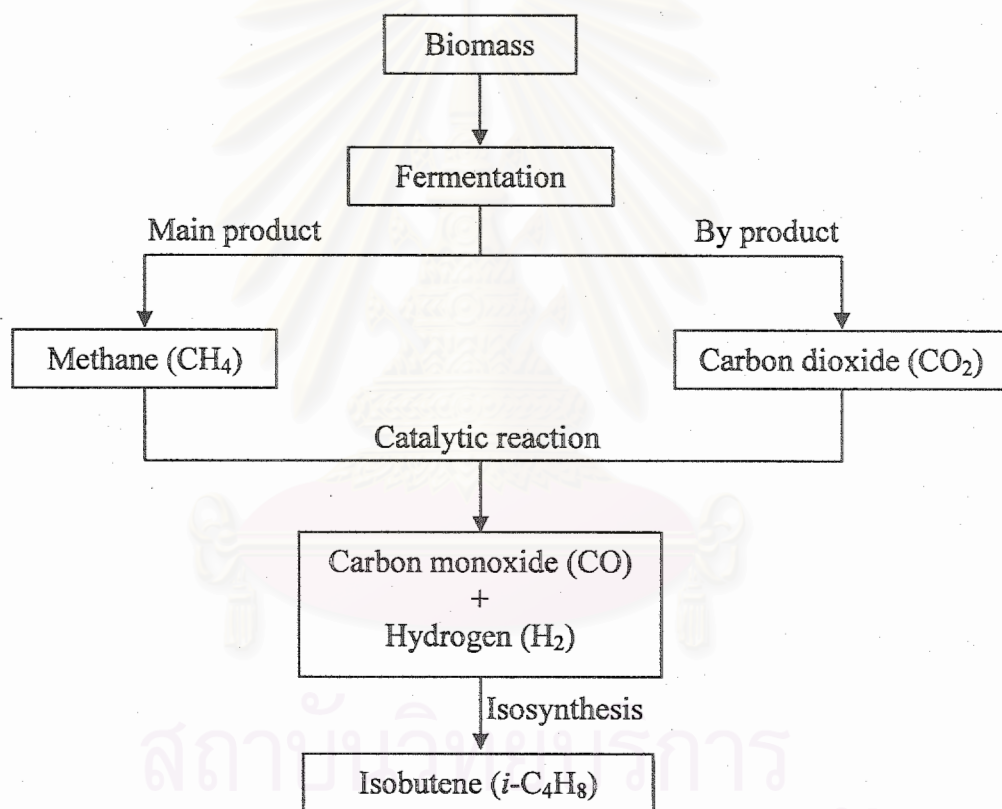
Figure 1.1 Isobutene synthesis from renewable resource

Some researchers have tried to relate the characteristics of catalysts to their catalytic performance. For example, Su *et al.* (2000) have investigated the catalytic performance of various nanoscale zirconias for isosynthesis. In addition, effect of the crystal phase such as monoclinic phase in zirconia on the catalytic performance was also reported by Maruya *et al.* (2000). Because of the bifunctionality of zirconia, the acid-base properties could play an important role on the catalytic performance (Su *et*

2

al., 2000, Li *et al.*, 2001, Li *et al.*, 2002, Li *et al.*, 2004). Therefore, there are many factors affecting the catalytic performance.

In this work, other factors such as the crystallite size of catalysts and Zr^{3+} on the catalyst surface are investigated. Moreover, the mixed oxide catalysts prepared by coprecipitation and physical mixing method are also studied.

The objectives of this research are as follows:

1. To investigate the characteristics and the catalytic properties of various ZrO_2 and CeO_2 catalysts during isosynthesis.
2. To investigate the effect temperature ramp during calcination of ZrO_2 on catalytic performance.

CHAPTER II

THEORY

This chapter focuses on carbon monoxide hydrogenation reactions particularly Fischer-Tropsch synthesis (FTS) and isosynthesis. It consists of five main sections. Details of Fischer-Tropsch synthesis (FTS) and isosynthesis are described in Sections 2.1 and 2.2, respectively. General features of zirconia and ceria, the main catalysts used in this study, are detailed in Sections 2.3 and 2.4, respectively. Finally, the preparation method of catalysts is explained in Section 2.5.

2.1 Fischer-Tropsch synthesis (FTS)

Fischer-Tropsch synthesis (FTS) or CO hydrogenation reaction is an important reaction for production of liquid hydrocarbons from synthesis gases (CO and H_2). During the past decades, FTS has been developed continuously by many researchers, although the rise and fall in research intensity on this process has been highly related to demands for liquid fuels and relative economics. This synthesis is basically the reductive polymerization (oligomerization) of carbon monoxide by hydrogen to form organic products containing mainly hydrocarbons and some oxygenated products in lesser amounts. The main reactions of FTS are:

$$CO + 3H_2 \rightarrow CH_4 + H_2O \qquad (2.1)$$

$$CO + 2H_2 \rightarrow (\frac{1}{n})(C_nH_{2n}) + H_2O \qquad (2.2)$$

$$CO + H_2O \rightarrow CO_2 + H_2 \qquad (2.3)$$

$$2CO \rightarrow C + CO_2 \qquad (2.4)$$
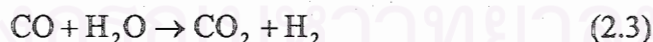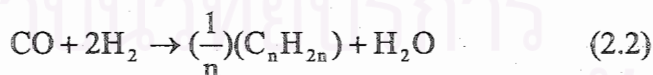
Equation (2.1) is the formation of methane, Equation (2.2) is the synthesis of hydrocarbons higher than methane, Equation (2.3) is the water-gas shift reaction, and Equation (2.4) is the Boudouard reaction resulting in deposition of carbon.

4

The current main goal in FTS is to obtain high molecular weight, straight chain hydrocarbons. However, methane and other light hydrocarbons are always present as less desirable products from the synthesis. According to the Anderson-Schulz-Flory (ASF) product distribution, typically 10 to 20% of products from the synthesis are usually light hydrocarbons (C_1-C_4). These light alkanes have low boiling points and exist in the gas phase at room temperature, which is inconvenient for transportation. Many attempts have been made to minimize these by-products and increase the yield of long chain liquid hydrocarbons by improving chain growth probability. It would be more efficient to be able to convert these less desirable products into more useful forms, rather than re-reforming them into the synthesis gas and recycling them (Farrauto and Bartholomew, 1997). Depending upon the type of catalyst used, promoters, reaction conditions (pressure, temperature and H_2/CO ratios), and type of reactors, the distribution of the molecular weight of the hydrocarbon products can be noticeably varied.

2.2 Isosynthesis (Wender, 1996)

The isosynthesis is part of the more generalized reaction systems associated with the Fischer-Tropsch process. This synthesis gas reaction was developed during World War II by Pichler and Ziesecke (1949). Details of the project, actually started in 1941, were kept secret because its primary goal was the catalytic production of isobutane and isobutene, important raw materials for high octane gasoline syntheses (Pichler, 1952).

Synthesis gas is catalytically converted predominantly to branched hydrocarbons using certain difficultly reducible oxides as catalysts. Development of the process was rapid but its commercial use was cut off by the successful development of new catalysts for the production of high octane gasoline from readily available petroleum.

Although both isosynthesis and FTS use synthesis gas as the feed, the isosynthesis differs from the FTS in several ways

- The isosynthesis gives high yields of isoparaffins rather than normal paraffins.

5

- The catalysts are difficultly reducible oxides such as ThO_2 or ZrO_2 rather than reduced transition metals.

- Isosynthesis temperatures and pressures are considerably higher than those used in FTS.

- Isosynthesis catalysts are not poisoned by sulfur to any great extent.

Very few efforts have been reported about the isosynthesis process since the early work by Pichler and Ziesecke (1949), but interest in this reaction has been revived, chiefly because of the growing demand for isobutene and other branched hydrocarbons. Sofianos (1992) has reviewed the synthesis. The existing literature seems to reveal that the main products of the isosynthesis reaction, namely isobutene and isobutane, can be obtained in sufficiently high yields only at high temperatures and pressures. The operation of the isosynthesis reaction is not favorable at low pressures as the formations of DME, lower alcohols and isobutanol predominate under these conditions.

Isobutanol was one of the main products of Pichler and Ziesecke's isosynthesis reaction, indicating a relationship between the Isosynthesis and the higher alcohol synthesis. Isobutanol and other higher alcohols can be produced using a number of catalytic systems under milder conditions with greater yields than iso-C_4 compounds from the Isosynthesis. Large amount of methanol is always present and it becomes a driving force to realize a direct reaction between methanol and isobutanol or isobutene derived from isobutanol to form MTBE.

A large number of reactions taking place during the FTS reaction or isosynthesis can be summarized as follows:

Paraffins $$(2n+1)H_2 + nCO \rightarrow C_nH_{2n+2} + nH_2O \qquad (2.5)$$

Olefins $$2nH_2 + nCO \rightarrow C_nH_{2n} + nH_2O \qquad (2.6)$$

Alcohols $$2nH_2 + nCO \rightarrow C_nH_{2n+1}OH + (n-1)H_2O \qquad (2.7)$$

Water gas shift $$CO + H_2O \rightarrow CO_2 + H_2 \qquad (2.8)$$

Boudouard reaction $$2CO \rightarrow C + CO_2 \qquad (2.9)$$

Coke deposition $H_2 + CO \rightarrow C + H_2O$ (2.10)
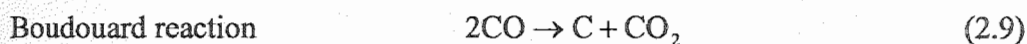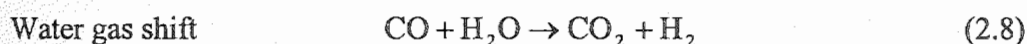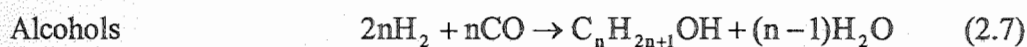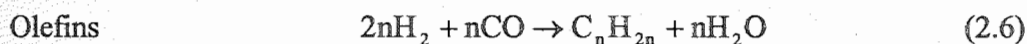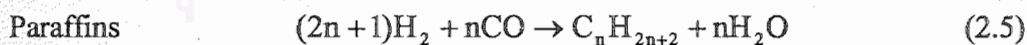
Noted that the best yields are obtained with a CO: H_2 ratio of 1.0 - 1.2: 1.0.

2.3 General feature of zirconia

It has been reported that zirconia forms three different phases: monoclinic, tetragonal, and cubic. Figure 2.1 shows the typical unit cells of different phases. Crystal structures of cubic, tetragonal and monoclinic zirconia are shown in Figure 2.2. The monoclinic is stable up to ca. 1170°C, at which temperature transforms into the tetragonal phase, which is stable up to 2370°C (Cormack and Parker, 1990). The stabilization of the tetragonal phase below 1100°C is important in the use of zirconia as a catalyst in some reactions. Above 2370°C, the cubic phase is stable and exists up to the melting point of 2680°C. Due to the martensitic nature of the transformations, neither the high temperature tetragonal nor cubic phase can be quenched in rapid cooling to room temperature. However, at low temperature, a metastable tetragonal zirconia phase is usually observed when zirconia is prepared by certain methods, for example by precipitation from aqueous salt solution or by thermal decomposition of zirconium salts. This is not the expected behavior according to the phase diagram of zirconia (i.e., monoclinic phase is the stable phase at low temperatures). The presence of the tetragonal phase at low temperatures can be attributed to several factors such as chemical effects, (the presence of anionic impurities) (Srinivasan et al., 1990, Tani et al., 1982) structural similarities between the tetragonal phase and the precursor amorphous phase (Livage et al., 1968, Osendi et al., 1985, Tani et al., 1982) as well as particle size effects based on the lower surface energy in the tetragonal phase compared to the monoclinic phase (Garvie, 1978, Osendi et al., 1985, Tani et al., 1982). The transformation of the metastable tetragonal form into the monoclinic form is generally complete by 650-700°C.

Crystal system	Unit cell shape
Cubic	$a = b = c, \alpha = \beta = \gamma = 90°$
Tetragonal	$a = b \neq c, \alpha = \beta = \gamma = 90°$
Monoclinic	$a \neq b \neq c, \alpha = \gamma = 90°, \beta \neq 90°$
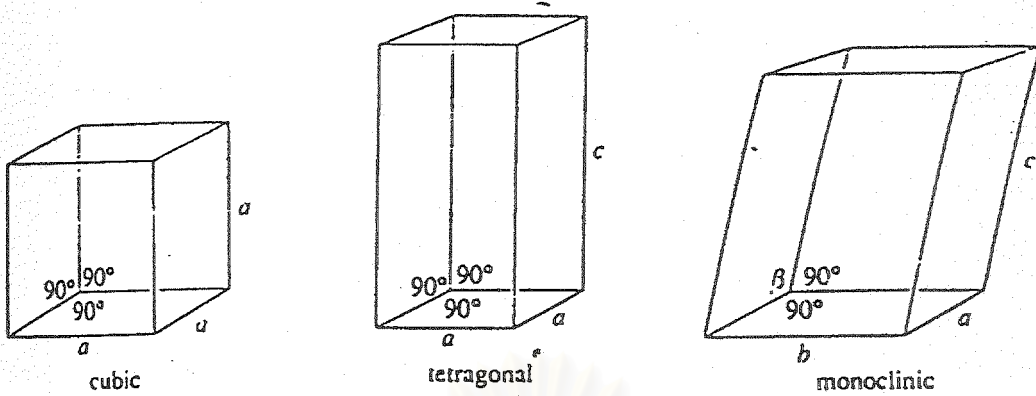
Figure 2.1 The unit cells of the crystal systems (West, 1997).
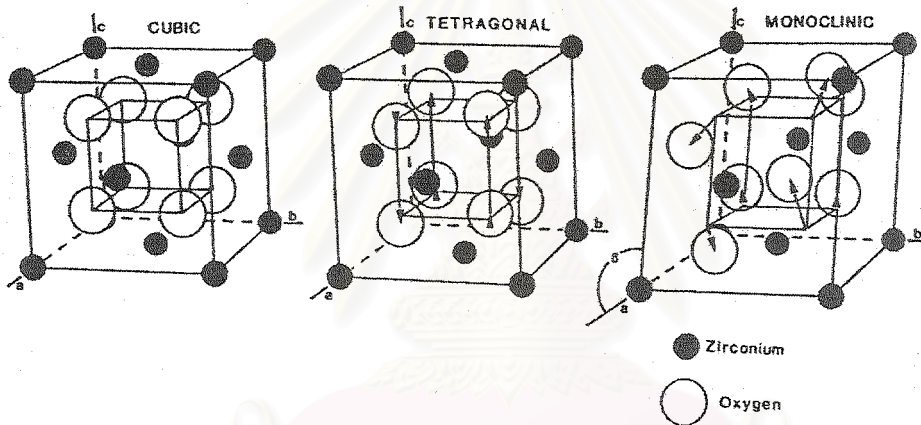
Figure 2.2 Crystal structure of cubic, tetragonal and monoclinic zirconia (Heuer, 1987).

2.4 Cerium dioxide

2.4.1 Physical and Chemical Properties

The band gap energy of cerium dioxide or ceria (CeO_2) with the cerianite or fluorite structure is 2.95 eV, being able to filter out UV rays less than 400 nm in wavelength (Sato *et al.*, 2004). CeO_2 has interesting economical and physicochemical

properties. Cerium dioxide is abundant, nontoxic and inexpensive. Furthermore, CeO_2 is a semi-conducting material that absorbs light in the near UV and slightly in the visible region. These features make cerium dioxide a promising material that can be used in heterogeneous photocatalytic reactions. Other selected properties of cerium dioxide are given in Table 2.1.

Table 2.1 Selected physicochemical properties of cerium dioxide (Bamwenda and Arakawa, 2000).

Properties	Value
Color	Yellowish-white
Density	7.1 g cm^{-3}
Surface area	~9.5 m^2 g^{-1}
Acidity	Weak base
$\Delta H_f^o{}_{298}$	-246 kcal mol^{-1}
T $_{melting}$	2873 K
Crystal system	face-centered cubic
Electronegativity	2.3 pauling
Absorption edge	~420 nm
Bandgap[a]	~2.95 eV
Conductivity	1.2-2 x 10^{-8} Ω^{-1} cm^{-1}

[a] The bandgap was estimated from the plot of the UV-VIS absorption vs λ following the equation, $E_{BG} = 1240/\lambda_{onset}$.

2.4.2 Applications of Cerium dioxide

CeO_2 is widely employed in sun care products and an oxygen storing component in automotive three-way catalysts. In practice, ceria is frequently used in combination with other oxides. Cerium dioxide containing materials have been the subject of numerous investigations in recent years because of their very broad range of applications in catalysis and in advanced ceramic materials. The success of ceria in diverse applications is mainly due to its unique combination of an elevated oxygen transport capacity coupled with the ability to shift easily between reduced and oxidized state ($Ce^{3+} \leftrightarrow Ce^{4+}$). In particular, supported ceria and CeO_2-based mixed oxides are the effective catalysts for the oxidation reactions of different hydrocarbons and for the removal of total organic carbon from polluted water from different sources. It is used in various catalytic reactions such as CO_2 activation, CO oxidation, CO/NO removal. Despite its widespread applications, the use of pure cerium dioxide is highly discouraged because it is poorly thermostable as it undergoes sintering at high temperature, thereby losing its crucial oxygen storage and release characteristics. Nowadays, CeO_2 can be used as a material for photocatalyst in the photooxidation of water and other VOCs (Bamwenda and Arakawa, 2000).

2.5 Preparation method of catalysts

2.5.1 Precipitation and Coprecipitation (Ertl *et al.*, 1997)

The preparation of catalyst and support by precipitation or coprecipitation is technically very important (Thomas, 1970 and Stiles, 1983). However, precipitation is usually more demanding than several other preparation techniques, due to the necessity of product separation after precipitation and the large volumes of salt-containing solutions generated in precipitation processes. Techniques for catalyst manufacture thus have to produce catalysts with better performance in order to compensate for the higher cost of production in comparison, for instance, to solid-state reactions for catalyst preparation.

Nevertheless, for several catalytically relevant materials, especially for support materials, precipitation is the most frequently applied method of preparation. These materials include mainly aluminum and silicon oxides. In other systems precipitation techniques are also used, for instance in the production of iron oxides, titanium oxides or zirconias. The main advantages of precipitation for the preparation of such materials are the possibility of creating very pure materials and the flexibility of the process with respect to final product quality.

Other catalysts, based on more than one component, can be prepared by coprecipitation. According to IUPAC nomenclature, coprecipitation is the simultaneous precipitation of a normally soluble component with a macrocomponent from the same solution by formation of mixed crystals, by adsorption, occlusion or mechanical entrapment. However, in catalyst preparation technology, the term is usually used in a more general sense in that the requirement of one species being soluble is dropped. In many cases, both components to be precipitated are essentially insoluble under precipitation conditions, although their solubility products might differ substantially. We will therefore use the term coprecipitation for the simultaneous precipitation of more than one component. Such systems prepared by coprecipitation include Ni/Al_2O_3, Cu/Al_2O_3, Cu/ZnO, and Sn-Sb oxides.

Coprecipitation is very suitable for the generation of a homogeneous distribution of catalyst components or for the creation of precursors with a definite stoichiometry, which can be easily converted to the active catalyst. If the precursor for the final catalyst is a stoichiometrically defined compound of the later constituents of the catalyst, a calcination and/or reduction step to generate the final catalyst usually creates very small and intimately mixed crystallites of the components. Such a good dispersion of catalyst components is difficult to achieve by other means of preparation, and thus coprecipitation still remains an important technique in the manufacture of heterogeneous catalysts in spite of the disadvantages associated with such processes. These disadvantages are the higher technological demands, the difficulties in following the quality of the precipitated product during the precipitation, and the problems in maintaining a constant product quality throughout the whole precipitation process, if the precipitation is carried out discontinuously.

2.5.1.1 General Principles Governing Precipitation from Solutions

Precipitation processes are not only relevant for catalysis, but also for other industries, as for instance the production of pigments. However, in spite of the tremendous importance of precipitation from solution, many basic questions in this field are still unsolved and the production of a precipitate with properties that can be adjusted at will is still rather more an art than a science. This is primarily due to the fact that the key step, nucleation of the solid from a homogeneous solution, is a very elusive one, and is difficult to study using the analytical tools currently available.
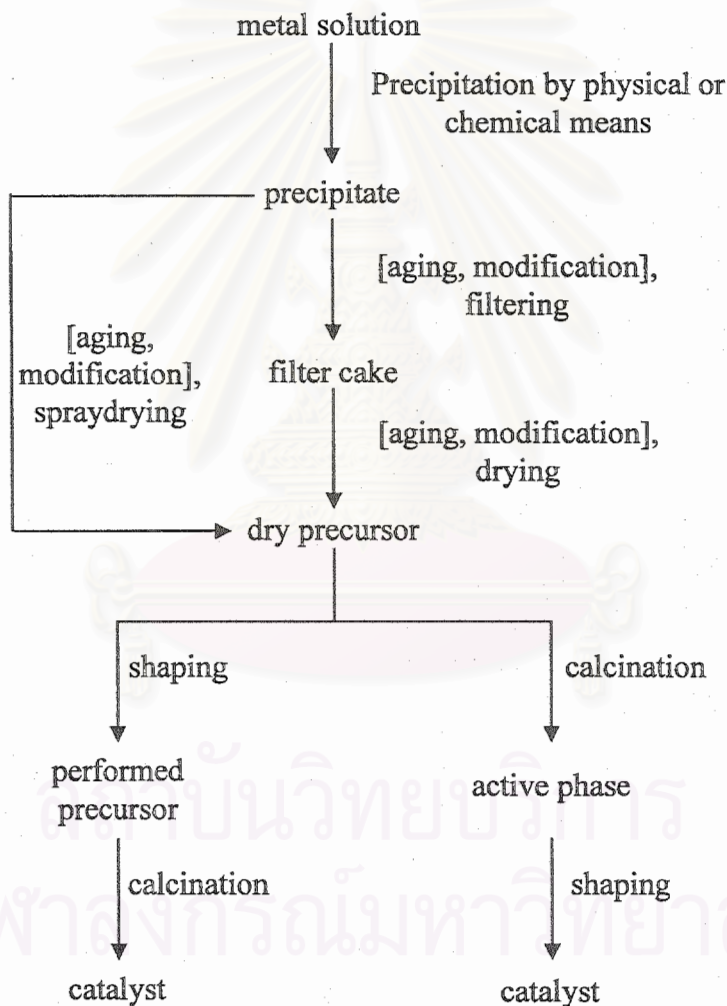
Figure 2.3 Preparation scheme for precipitated catalysts (optional preparation steps are indicated by square brackets).

Spectroscopy using local probes is not sensitive enough to study larger arrangements of atoms on the one hand. In addition, diffraction methods are not suitable for analysis either, since a nucleus is not large enough to produce a distinctive diffraction pattern. Thus, investigations of crystallization and precipitation processes from solution often have to rely on indirect and theoretical methods. Figure 2.3 depicts a general flow scheme for the preparation of a precipitated catalyst.

2.5.1.2 Chemical Considerations

It is generally desirable to precipitate the desired material in such a form, that the counter-ions of the precursor salts and the precipitation agent, which can be occluded in the precipitate during the precipitation, can easily be removed by a calcination step. If precipitation is induced by physical means, i.e. cooling or evaporation of solvent to reach super-saturation of the solution, only the counter-ion of the metal salt is relevant. If precipitation is induced by addition of a precipitating agent, ions introduced into the system via this route also have to be considered. Favorable ions are nitrates, carbonates, or ammonium, which decompose to volatile products during the calcination. For catalytic applications usually hydroxides, oxohydrates, oxides (in the following the term "hydroxides" is used in a rather general sense, comprising hydroxides and oxides with different degrees of hydration) are precipitated; in some cases carbonates, which are subsequently converted to the oxides or other species in the calcination step, are formed. In addition, the precipitation of oxalates as precursors for spinel-type catalysts has occasionally been reported to give good results (Peshev *et al.*, 1989). If the ions do not decompose to volatile products, careful washing of the precipitate is necessary.

In many cases it has been found advantageous to work at low and relatively constant super-saturation which is achieved homogeneously in the whole solution (precipitation from homogeneous solution, PFHS). This can also be employed for deposition-precipitation processes. This can be reached by using a precipitating agent which slowly decomposes to form the species active in the precipitation.

13

2.5.1.3 Process Considerations

There are several ways to carry out the precipitation process (Figure 2.4) (Courty and Marcilly, 1983). The simplest implementation of the precipitation reaction is the batch operation where the solution from which the salt is to be precipitated is usually present in the precipitation vessel and the precipitating agent is added. The advantage of this mode of operation is the simple way in which the product can be obtained; the most severe disadvantage is the variation of batch composition during the precipitation process. This can lead to differences between the product formed during the initial stages of the precipitation and the precipitate formed at the end of process. If a coprecipitation is carried out this way, it is important to decide which compounds are present in the vessel and which compounds are to be added. If the precipitating agent is present in the precipitator and the mixed metal solutions are added, the product tends to be homogeneous, since the precipitation agent is always present in large excess. If, on the other hand, the precipitating agent is added to a mixed metal solution, the precipitate with the lower solubility tends to precipitate first, thus resulting in the formation of an inhomogeneous product.

A slightly more complex process is the simultaneous addition of both reagents under strict control of the pH and the reagent ratios. If the precipitation is carried out following this procedure, the ratio of the metal salt and precipitating agent remains constant; all other concentrations, however, change during the process. Homogeneity of the product is usually better than in the first process described, but might still vary between the first precipitate and the precipitate formed last. This is due to the different concentrations of the other ions which are not precipitated and might be occluded in the precipitate to a larger extent during the final stages of the procedure. Moreover, the precipitates first formed are aged for a longer time in the solution. Thus, phase transitions might have already occurred, while fresh precipitates are still formed.

a: Batchwise operation   b: Batchwise operation with constant pH

c: Continuous operation
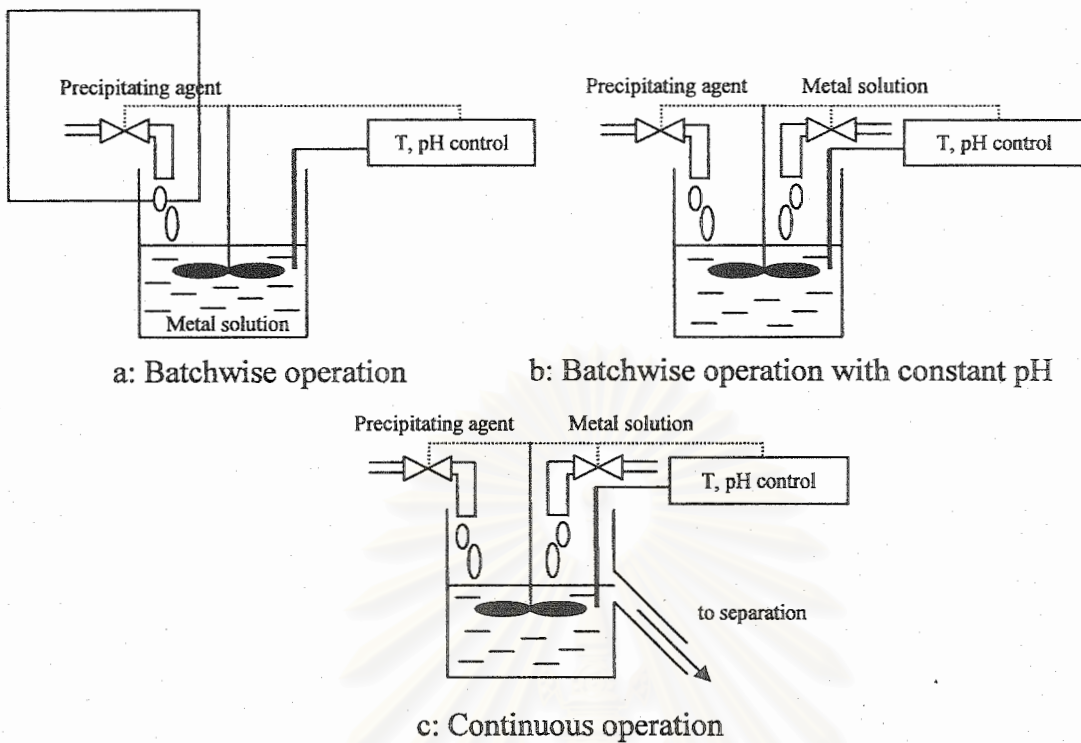
Figure 2.4 Possible implementations of precipitation processes.

Note that in the batchwise process (a) the pH and all other parameters except for the temperature change continuously during the precipitation due to consumption of the metal species. Coprecipitation should be carried out in the reversed arrangement by addition of the metal species to the precipitating agent to avoid sequential precipitation. In process (b) the pH is kept constant, but the batch composition and the residence time of the precipitate change continuously. In process (c) all parameters are kept constants.

These problems are avoided if a continuous process is employed for the precipitation; however, this makes higher demands on the process control. In a continuous process all parameters as temperature, concentrations, pH, and residence times of the precipitate can be kept constant or altered as desired.

The continuous process usually allows precipitation at low supersaturation conditions, since seeds are already present in the precipitation vessel. Thus, no homogeneous precipitation, which needs high levels of super-saturation, is necessary,

and nucleation occurs heterogeneously with the associated lower supersaturation levels.

2.5.1.4 Influences on Properties of the Final Product

Basically all process parameters, some of which are fixed and some which are variable, influence the quality of the final product of the precipitation. Usually precipitates with specific properties are desired. These properties could be the nature of the phase formed, chemical composition, purity, particle size, surface area, pore sizes, pore volumes, separability from the mother liquor, and many more, including the demands which are imposed by the requirements of downstream processes, like drying, palletizing, or calcination. It is therefore necessary to optimize the parameters in order to produce the desired material. Figure 2.5 summarizes the parameters which can be adjusted in precipitation process and the properties which are mainly influenced by these parameters. The following discussion attempts to give some general guidelines concerning the influence of certain process parameters on the properties of the resulting precipitate. It should, however, be stressed, that the stated tendencies are only trends which might vary in special cases. The exact choice of precipitation parameters is usually the result of a long, empirically driven optimization procedure and a well-guarded secret of catalyst manufacturers or the producers of precursors for catalysts.
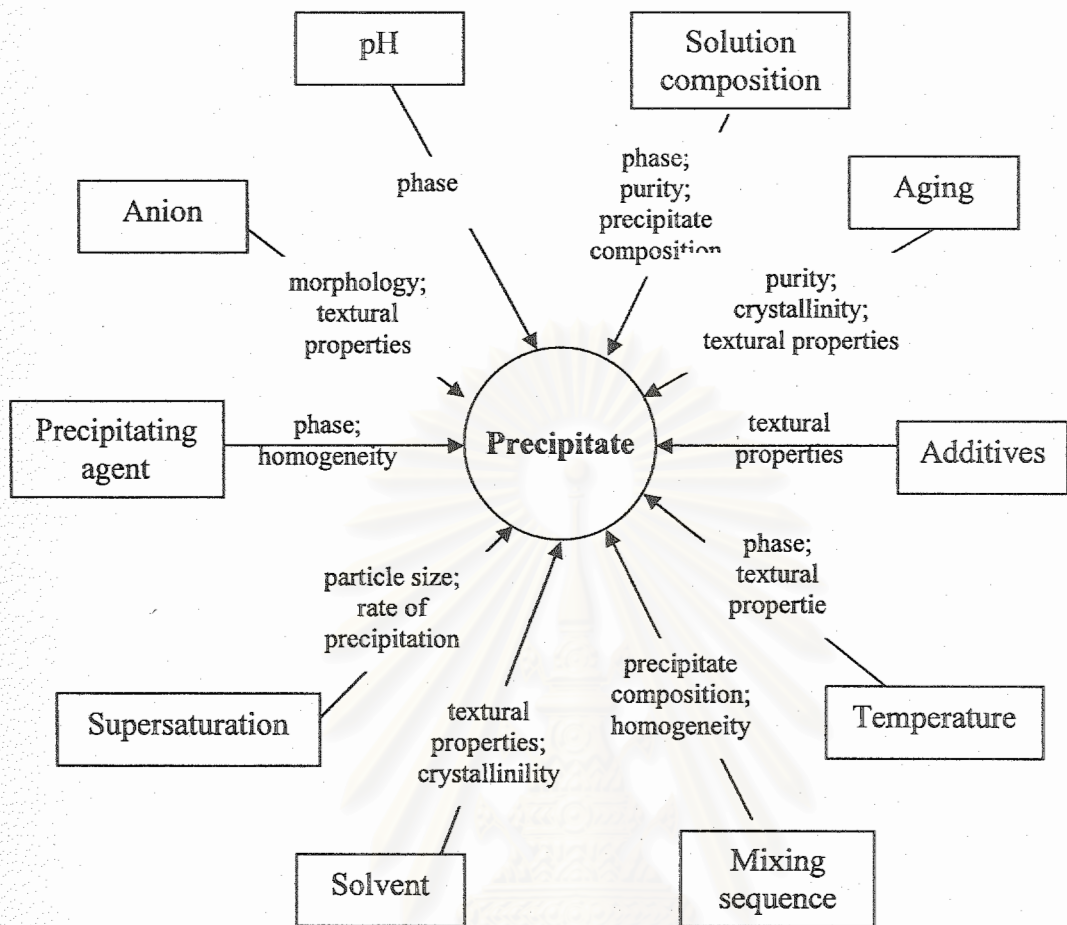
Figure 2.5 Parameters affecting the properties of the precipitate and main properties influenced.

CHAPTER III

LITERATURE REVIEWS

3.1 Mechanism of isosynthesis over oxide catalysts

The chain-branching mechanisms for isobutene formation over ZrO_2 were proposed by early researchers (Ekerdt *et al.*, 1988 and 1990). The mechanisms consisted of two paths; (i) CO insertion into zirconium-carbon bond of adsorbed aldehydic intermediate and (ii) condensation between η-enolate and methoxide species. After that, Maruya *et al.* (1996) studied role of methoxide species over ZrO_2 for isobutene formation. The results indicated that methoxide species were important to form isobutene. They proposed the reaction path consisting of (i) conversion of methoxide species to η^2-formaldehyde species, (ii) formation of methyl or methylene species from the η^2-formaldehyde species by hydrogenation or thermolysis, (iii) carbonylation of the methyl or methylene species to form C_2 oxygenate, (iv) aldol-condensation type reaction to form branched C_4 oxygenates, and (v) formation of branched hydrocarbons from the hydrogenation followed by dehydration. Moreover, Maruya *et al.* (1998) investigated the procedure of transformation of methoxy species to isobutene over oxide catalysts such as ZrO_2, CeO_2, ZrO_2-CeO_2, ZrO_2-CeO_2-CoO and ZrO_2-CeO_2-Fe_2O_3. Reactions were carried out in a conventional flow system at 643 K, atmospheric pressure, a H_2/CO ratio of 1 and amount of catalysts of 2 g. The results from the experiments revealed that paths of the selective formation to isobutene over oxide catalysts were: (1) formation of methoxy species from CO and H_2, (2) conversion of methoxy species to methyl species, (3) insertion of CO into a methyl-metal bond, and (4) aldol condensation of C_2 oxygenates with formaldehyde. Furthermore, the presence of dimethyl ether (DME) in the CO hydrogenation products caused the different selectivity of isobutene. ZrO_2, ZrO_2-CeO_2 and ZrO_2-CeO_2-CoO offered high isobutene selectivity in C_4 hydrocarbons of about 92-97%, CeO_2 showed almost no isobutene selectivity. ZrO_2-CeO_2-Fe_2O_3 offered lower isobutene but higher methane selectivity.

3.2 Effect of preparation of oxide catalysts

3.2.1 Precipitation method

Many previous researchers prepared zirconia by precipitation method, which was carried out by adding a solution of zirconium salt precursors such as zirconyl chloride ($ZrOCl_2$) to a well-stirred precipitating solution (e.g. NH_4OH, KOH, or NaOH), which was normally ammonium hydroxide, at room temperature. The pH of the solution was controlled at 10 (Li *et al.*, 2001, Li *et al.*, 2002, Li *et al.*, 2003, Li *et al.*, 2004, Su *et al.*, 2000). The resulting precipitate was removed, and then washed with deionized water until chloride ion (Cl^-) was not detected with silver nitrate ($AgNO_3$) solution. The obtained sample was dried overnight and then calcined.

Maruya *et al.* (2000) investigated influence of phase structure and active sites over ZrO_2 on the selective formation of isobutene. Reactions were carried out using a conventional flow system at 673 K, atmospheric pressure, a H_2/CO ratio of 1 and amount of catalysts of 2 g. It was reported that fraction of monoclinic phase on ZrO_2 catalysts was dependent on pH value of precipitation. The rate of isobutene formation increased with an increase in the volumetric fraction of monoclinic phase, while formation of the other hydrocarbons was independent of the fraction. Selectivity of isobutene in C_4 hydrocarbons and total hydrocarbons for precipitation pH range of 7.0-10.5 were 94 and 77%, respectively. The amounts of methoxy and formate species as well as the surface sites with strong basicity increased with an increase in the fraction of monoclinic phase. Moreover, the effectiveness of monoclinic structure was attributed to the unsaturation of coordination sites, which were assumed to be effective for the formation of methoxy species, and the strong basicity, which was available for formation C_3 hydrocarbons from the C_2 oxygenate and branched C_4 compounds from C_3 oxygenate.

Furthermore, the other preparation based methods such as supercritical fluid drying (SCFD) and freeze-drying (FD) for preparing ZrO_2 catalysts were performed by Su *et al.* (2000), who studied nanosize zirconia catalysts. Reactions were carried out using a flow-type fixed-bed pressurized tubular reactor at 673 K, 5.0 MPa, a H_2/CO ratio of 1 and amount of catalysts of 2 g. The drying conditions of these

preparation methods affected the crystal, acidic and basic properties of nanosize zirconia. The results showed that the highest selectivity of isobutene in total hydrocarbons was obtained over nanosize zirconia prepared by precipitation method.

Furthermore, Su *et al.* (2000) studied influences of preparation parameters, such as precipitation pH, zirconium salt precursors and calcination temperatures, on the characteristic and catalytic performance of zirconia catalysts. The results exhibited that the catalytic performance of zirconia was strongly influenced by those parameters, but, the crystal phase of zirconia was not dependent on the pH, unlike the results of Maruya *et al.* (2000). When the pH was changed in the range of 6-14, the main crystal phase was always monoclinic. Zirconia was precipitated at pH 6-7. The highest activity of CO was about 80%, while the selectivity of isobutene in C_4 hydrocarbons and total hydrocarbons were only 36 and 7.5%, respectively. However, zirconia precipitated at pH varying from 3 to 10 was the most selective to the formation of isobutene. The selectivity of isobutene in C_4 hydrocarbons and total hydrocarbons were 100 and 59.6%, respectively, however, the activity was merely 16%. For different zirconium salt precursors, it was found that trace amount of SO_4^{2-} strongly affects the structure and catalytic performance of the catalysts. Zirconia calcined at 873 K showed the highest selectivity of isobutene of about 55% in total hydrocarbons.

3.2.2 Mechanical mixing method

In the mechanical mixing method, ZrO_2-based catalysts were prepared by using calcined zirconia obtained from precipitation method and promoters, such as Al_2O_3, KOH and calcium salts. The promoters were milled together with ZrO_2 thoroughly and then the mixture was calcined again.

Based on the mechanical mixing method, Li *et al.* (2001) studied the promoting effects of various calcium salts on isosynthesis over ZrO_2 catalysts. Reactions were carried out in a fixed-bed flow type pressurized stainless steel tubular reactor in the temperature range of 673-723 K, pressure of 5.0 MPa, a H_2/CO ratio of 1 and amount of catalysts of 2.1 g. Calcium salts added into zirconia was reported to influence catalytic performance. The results indicated that the additions of CaF_2 and

CaSO$_4$ into zirconia could remarkably enhance the selectivity of i-C$_4$ in total hydrocarbons from 40 up to 50% while maintaining the activity of pure ZrO$_2$ at 18%. Moreover, Li et al. (2002) investigated influence of acidic and basic properties of ZrO$_2$ based catalysts with calcium salts, Al$_2$O$_3$ and KOH as promoters on isosynthesis. The experimental results indicated that the promoters affected both the amount of acid-base sites and the strength of acid and base catalysts as well as activity and selectivity of isosynthesis. From the results, Al$_2$O$_3$-KOH were effective promoters, which could remarkably enhance i-C$_4$ selectivity in total hydrocarbons from 40 up to 65% while maintaining the activity as pure ZrO$_2$ at 18%.

3.2.3 Coprecipitation method

The mixed oxides, which were zirconia based catalysts, were synthesized by coprecipitation of a mixed solution of zirconium salt precursor, such as ZrOCl$_2$, and various additives, such as cerium or yttrium nitrate salts, with ammonium solution. Li et al. (2004) applied the coprecipitation method to prepare ZrO$_2$-based catalysts doped with CeO$_2$ or Y$_2$O$_3$ and determined catalytic performance of the obtained catalysts. The activity and selectivity of the ZrO$_2$-based catalysts were reported to be varied with the quantity of CeO$_2$ and Y$_2$O$_3$ doped. The physical properties had no appreciable effects on the catalytic performance of the catalysts. The highest selectivity to i-C$_4$ in total hydrocarbons were 67 and 64% over 50% CeO$_2$-doped ZrO$_2$ and 8.6% Y$_2$O$_3$-doped ZrO$_2$, respectively.

3.3 Effect of reactor material

Apart from the properties of the catalysts, a reactor material is another factor that influenced catalytic performance of the system. Li et al. (2003) compared the isosynthesis performance of two reactors made from stainless steel and quartz. The catalysts were Al$_2$O$_3$ and several calcium salts promoted ZrO$_2$-based prepared by mechanical mixing method. The results demonstrated that the stainless steel tubular reactor seriously affected the selectivity of isosynthesis, while the quartz reactor that could eliminate the influence of the metal wall of the stainless steel was favorable for i-C$_4$ hydrocarbons formation and especially, for suppressing the formation of CO$_2$ that was main by-product. The selectivity of i-C$_4$ in total hydrocarbons increased from 40

to 53% and CO_2 formation decreased from 47 to 38%. Al_2O_3 which was added into ZrO_2 could largely enhance the activity while maintaining i-C_4 selectivity as high as pure ZrO_2. The addition of CaF_2 or $CaSO_4$ into ZrO_2 exhibited high i-C_4 formation but still maintained the activity of pure ZrO_2. Moreover, from the study of the influence of reaction temperatures on the catalytic performance of the catalysts, it was found that the suitable reaction temperatures for i-C_4 formation were about 673-698 K.

3.4 Effect of acidic and basic properties

Several researches were conducted to investigate the effect of acidic and basic properties on catalytic performance in the isosynthesis. The acidic and basic properties of the catalysts were studied by temperature-programmed desorption (TPD) of NH_3 and CO_2, respectively. Report of Su et $al.$ (2000) suggested that both the acid and base sites on the catalysts are required for the isosynthesis when adding acidic and basic components into zirconia. The activity was increased by adding acidic component into zirconia and the selectivity of isobutene was increased largely by adding basic component into zirconia. Furthermore, Li et $al.$ (2002, 2004) suggested that the acidic sites are responsible for the activation of reactant molecules (or activity) and the formation of linear C_4 hydrocarbons, and basic sites of the catalysts are significant for the formation of isobutene. Higher ratios of basic to acidic sites led to higher selectivity of isobutene. The ratio of base to acid sites on the catalysts would determine the percentage of n-C_4 and i-C_4 in total C_4 hydrocarbons.

3.5 Effect of redox properties

Li et $al.$ (2004) studied effects of redox properties and acid-base properties on isosynthesis over ZrO_2-based catalysts doped with CeO_2 or Y_2O_3 which were prepared by coprecipitation method. The addition of CeO_2 or Y_2O_3 into ZrO_2 enhanced the reduction properties of the catalysts as shown from temperature-programmed reduction (TPR) measurements. The highest activity and, C_4 and i-C_4 selectivity in total hydrocarbons were obtained over the catalysts which have a maximum amount of H_2 consumption measured by TPR for both CeO_2- and Y_2O_3-

doped ZrO_2-based catalysts. In addition, the acid-base properties also played a significant role in determining the activity and selectivity of the catalysts.

CHAPTER IV

EXPERIMENTS

This chapter describes experimental systems and procedures used in this work. It is divided into three sections including catalyst preparation, catalyst characterization and reaction study for isosynthesis via CO hydrogenation.

Catalyst preparation methods for ZrO_2, CeO_2, coprecipitated and physically mixed ZrO_2-CeO_2 catalysts are described in Section 4.1. The next section (Section 4.2) explains catalyst characterization techniques consisting of XRF, N_2 physisorption, XRD, TPD, ESR and Electron microscopy (SEM/EDX). Finally, the catalytic performance measurement in isosynthesis is illustrated in Section 4.3.

4.1 Catalyst Preparation

4.1.1 Chemicals

1. Ammonium hydroxide from Aldrich.
2. Zirconyl nitrate hydrate from Aldrich.
3. Zirconyl chloride, 30 % solution in hydrochloric acid from Aldrich.
4. Zirconium (IV) oxide, powder, < 5 micro from Aldrich.
5. Zirconium (IV) oxide, nanopowder from Aldrich.
6. Cerium (III) nitrate hexahydrate from Aldrich.
7. Cerium (IV) oxide, powder, < 5 micro from Aldrich.

4.1.2 Preparation of ZrO_2 and CeO_2 Catalysts

Zirconia (ZrO_2) was prepared by the precipitation method carried out by slowly adding a solution of zirconium salt precursors such as zirconyl chloride ($ZrOCl_2$) or zirconyl nitrate [$ZrO(NO_3)_2$] (0.15 M) into a well-stirred precipitating solution of ammonium hydroxide (NH_4OH) (2.5 wt%) at room temperature. The pH of the solution was carefully controlled at 10. The resulting precipitate was removed,

and then washed with deionized water until Cl⁻ was not detected by a silver nitrate $(AgNO_3)$ solution. The obtained sample was then dried overnight at $110^{\circ}C$ and calcined at $450^{\circ}C$ for 3 hours with a temperature ramp of $1^{\circ}C/min$. Moreover, the values of the temperature ramp were also varied at 2.5, 5.0, 7.5 and $10.0^{\circ}C/min$.

For the preparation of ceria (CeO_2), it was also prepared using the precipitation method as mentioned above. Cerium nitrate $[Ce(NO_3)_3]$ was used as a cerium salt precursor. All conditions during preparation were the same as those for the zirconia preparation.

4.2 Catalyst Characterization

4.2.1 X-ray Fluorescent Spectroscopy (XRF)

XRF was performed to determine composition in the bulk of catalysts. The analysis was performed using Siemens SRS3400 at Scientific Instruments Service centre, Faculty of Science, King Mongkut's Institute of Technology Ladkrabang.

4.2.2 N_2 Physisorption

Measurement of BET surface area, cumulative pore volume and average pore diameter were performed by N_2 physisorption technique using the Micromeritics ASAP 2020 surface area and porosity analyzer.

4.2.3 X-ray Diffraction (XRD)

The X-ray diffraction (XRD) patterns of powder were performed by X-ray diffractometer SIEMENS D5000 connected with a computer with Diffract ZT version 3.3 program for fully control of the XRD analyzer. The measurements were carried out using Ni-filtered CuK_{α} radiation. Scans were performed over the 2θ ranges of 20° - 80°. The crystallite size was estimated from line broadening according to the Scherrer equation and $\alpha-Al_2O_3$ was used as a standard. The calculation of crystallite

size was explained in Appendix A. In addition, the characteristic peaks of crystal phase from XRD spectra were used for calculating the fraction of crystal phase in catalyst as shown the example in Appendix B.

4.2.4 Temperature-programmed Desorption (TPD)

Temperature-programmed desorption techniques with ammonia and carbon dioxide (NH_3- and CO_2-TPD) were used to determine the acid-base properties of catalysts, respectively. TPD experiments were carried out using a flow apparatus. The catalyst sample (0.1g) was treated at its calcined temperature ($450^\circ C$) in helium flow for 1 hour and then saturated with 15% NH_3/He mixture or pure CO_2 flow after cooling to $100^\circ C$. After purging with helium at $100^\circ C$ for 1 hour to remove weakly physisorbed NH_3 or CO_2, the sample was heated to $450^\circ C$ at a rate of $20^\circ C$/min in a helium flow of 50 cm^3/min. The amount of acid-base sites on the catalyst surface was calculated from the desorption amount of NH_3 and CO_2, respectively. It was determined by measuring the areas of the desorption profiles obtained from the Micromeritics ChemiSorb 2750 Pulse Chemisorption System analyzer.

4.2.5 Electron Spin Resonance Spectroscopy (ESR)

Electron spin configuration was detected by using Electron spin resonance spectroscopy (ESR) (JEOL model JES-RE2X) at the Scientific and Technological Research Equipment Center, Chulalongkorn University (STREC). The sample was degassed before measurement at room temperature.

4.2.6 Electron Microscopy (SEM/EDX)

Scanning electron microscopy (SEM) and Energy dispersive X-ray spectroscopy (EDX) were used to determine the catalyst granule morphology and elemental distribution of the catalyst particles using JEOL JSM-5800LV scanning electron microscope. The SEM was operated using the back scattering electron (BSE) mode at 20kV. After the SEM micrographs were taken, EDX was performed to determine the elemental concentration distribution on the catalyst granules using Link

Isis Series 300 software at the Scientific and Technological Research Equipment Center, Chulalongkorn University (STREC).

4.3 Reaction Study in Isosynthesis via CO Hydrogenation

4.3.1 Materials

The reactant gases used for the reaction study were carbon monoxide (99.3%), ultra high purity hydrogen (99.999%) and high purity nitrogen (99.99%) supplied by Thai Industrial Gas Limited (TIG). The total flow rate was fixed at 25 cm^3/min with a CO: H$_2$: N$_2$ ratio of 10: 10: 5 cm^3/min, corresponding to a H$_2$/CO ratio of 1.

4.3.2 Apparatus

Flow diagram of a lab-scale gas phase isobutene synthesis system is shown in Figure 4.1. The system consisted of a reactor, an automatic temperature controller, an electrical furnace and a gas controlling system.

4.3.2.1 Reactor

The reactor was made from a quartz tube (O.D. 1/4"). Two sampling points were provided before and after the catalyst bed. Catalyst was placed between two quartz wool layers.

4.3.2.2 Automatic Temperature Controller

This unit consisted of a magnetic switch connected to a variable voltage transformer and a solid state relay temperature controller connected to a thermocouple. Reactor temperature was measured at the centre of the catalyst bed in

the reactor. The temperature control set point was adjustable within the range of 0-800°C at the maximum voltage output of 220 V.

4.3.2.3 Electric Furnace

The electric furnace with 2000 W heating coil was used to supply heat to the reactor for isosynthesis. The reactor could be operated from room temperature up to 600°C at the maximum voltage of 220 V.

4.3.2.4 Gas Controlling System

The controlling system for each gas consisted of a pressure regulator, an on-off valve and a mass flow controller.

4.3.2.5 Gas Chromatography

A gas chromatography Shimadzu model 8A (GC-8A) equipped with a thermal conductivity detector (TCD) was used to analyze compositions of carbon monoxide and hydrogen in the feed and product streams by using Molecular sieve column and used to analyze composition of carbon dioxide in the product stream by using Poropak-Q column. Hydrocarbons in the product stream were analyzed by a gas chromatography Shimadzu model 14B (GC-14B) equipped with a flame ionization detector (FID) by using VZ-10 column. The operating conditions for each instrument are listed in Table 4.1.

Table 4.1 Operating conditions for gas chromatography

Gas Chromatography	Shimadzu GC-8A		Shimadzu GC-14B
Detector	TCD		FID
Column - Column material - Length (m) - Outer diameter (mm) - Inner diameter (mm) - Mesh range - Maximum temperature (^{o}C)	Molecular sieve 5A SUS 2 4 3 60/80 350	Porapak-Q SUS 2 4 3 60/80 350	VZ-10 SUS 2 4 3 60/80 80
Carrier gas	Ar (99.999%)	Ar (99.999%)	N_2 (99.999%)
Carrier gas flow (ml/min)	30	30	30
Column temperature - initial (^{o}C) - final (^{o}C)	70 70	70 70	70 70
Injector temperature (^{o}C)	100	100	100
Detector temperature (^{o}C)	100	100	150
Current (mA)	70	70	-
Analyzed gas	N_2, H_2, CO	CO_2	Hydrocarbon C_1-C_4

4.3.3 Procedure

Experiments were carried out using a lab-scale isobutene synthesis system as shown in Figure 4.1. A catalyst (2 g) was packed in the middle of the quartz tube reactor located in the center of the electric furnace. The total flow rate was 25 cm^3/min with a H_2/CO ratio of 1. Isosynthesis was operated at 350-450 °C and atmospheric pressure.

The product gases were sampled to analyze the concentration of hydrocarbon (C_1-C_4) using GC-14B equipped with a VZ-10 column, whereas carbon monoxide and carbon dioxide concentration were analyzed by GC-8A equipped with Molecular sieve column and Porapak-Q column, respectively. The calibration curves of reactant (CO) and products (hydrocarbon C_1-C_4) are illustrated in Appendix C. Details of the calculation methods for determining catalytic activity to convert carbon monoxide, reaction rate and selectivity of product are given in Appendix D.
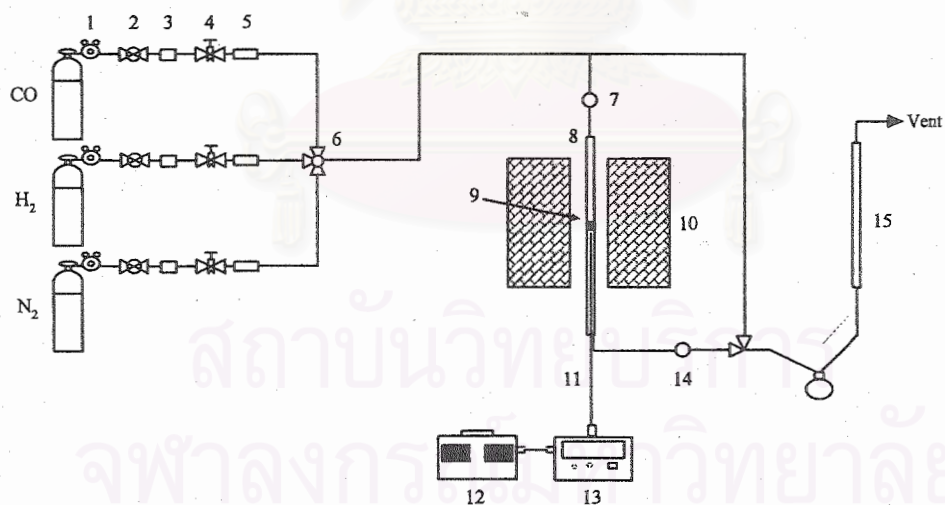
1. Pressure Regulator	2. On-Off Valve	3. Gas Filter
5. Back Pressure	6. 3-way Valve	7. Sampling Point
9. Catalyst Bed	10. Furnace	11. Thermocouple
13. Temperature Controller	14. Sampling Point	15. Bubble Flow Meter

Figure 4.1 Flow diagram of a lab-scale gas phase isobutene synthesis system.

CHAPTER V

RESULTS AND DISCUSSION

This chapter is divided into two sections. Comparison of catalytic properties of micron- and nanoscale ZrO_2 and CeO_2 catalysts is provided in Section 5.1. Effect of temperature ramp during calcination on characteristics of nanoscale ZrO_2 and its application as a catalyst for isosynthesis is discussed in Section 5.2.

5.1 Catalytic properties of micron- and nanoscale ZrO_2 and CeO_2 catalysts

In this section, ZrO_2 and CeO_2 catalysts were used for testing the catalytic performance on isosynthesis. The synthesized ZrO_2 obtained from $ZrOCl_2$ and $ZrO(NO_3)_2$ were denoted as ZrO_2-Cl (nano-syn) and ZrO_2-N (nano-syn), respectively. For CeO_2 prepared by $Ce(NO_3)_3$, it was denoted as CeO_2 (nano-syn). The commercial micron- and nanoscale ZrO_2 named as ZrO_2 (micron-com) and ZrO_2 (nano-com) and commercial micronscale CeO_2 named as CeO_2 (micron-com) obtained from Aldrich were also used for the comparative study.

5.1.1 Catalyst characterization

5.1.1.1 X-ray diffraction (XRD)

The XRD patterns of the commercial ZrO_2 and CeO_2 catalysts are shown in **Figure 5.1** and those of the synthesized ones are shown in **Figure 5.2**. They showed that both commercial and synthesized CeO_2 catalysts exhibited the similar XRD peaks at $2\theta = 28.6°$ and $33.1°$ assigned to the typical cubic fluorite structure. However, based on the calculation, it was found that the average crystallite size for the commercial CeO_2 was in microscale whereas the synthesized one was in nanoscale (**Table 5.1**). For the commercial microscale ZrO_2 catalyst (**Figure 5.1**), only the XRD peaks at $2\theta = 28.2°$ and $31.5°$ were observed, indicating the presence of the monoclinic phase only in the microscale ZrO_2. However, for the commercial nanoscale ZrO_2 catalyst (**Figure 5.1**), besides the monoclinic characteristic peaks it

also exhibited the XRD characteristic peaks of tetragonal phase at $2\theta = 30.2°$. For all catalysts, the contents of different phases are listed in **Table 5.1**. Typically, the monoclinic phase is stable up to ca. $1170°C$ and then, transforms into the tetragonal phase at higher temperature (Mercera *et al.*, 1991). The tetragonal phase is stable up to ca. $2370°C$ and finally transforms into the cubic phase at higher temperature. However, the metastable tetragonal phase in ZrO_2 can usually be observed when the precipitation method from an aqueous salt solution is employed as seen in this work or when the thermal decomposition of zirconium salts is used. Moreover, it was found that there was more tetragonal phase present in the nanoscale ZrO_2 compared with that in the micronscale one. The average crystallite size of each phase being present in all catalysts was calculated using the XRD line broadening regarding to its characteristic peaks. The micron- and nanoscale catalysts exhibited corresponding values based on their average crystallite sizes.
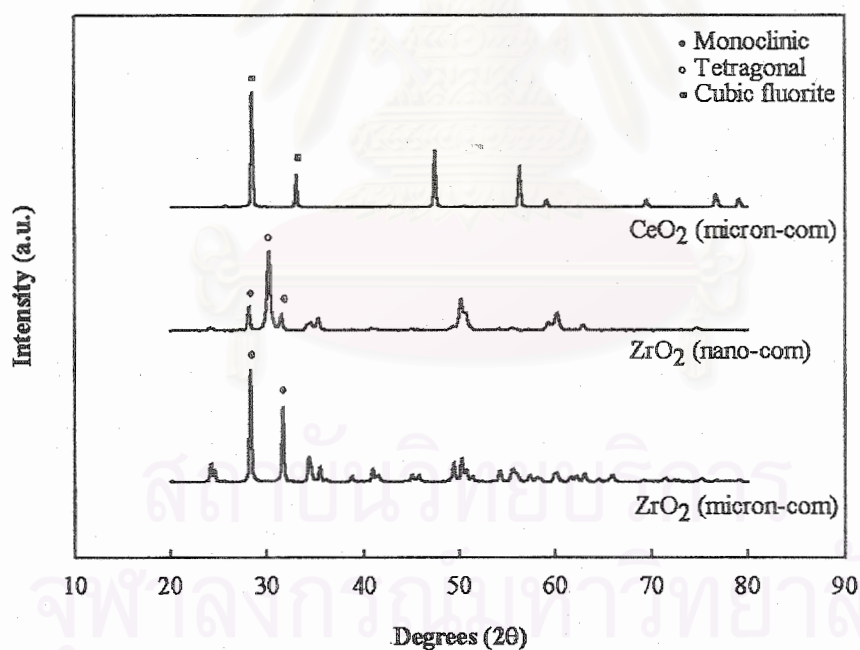
Figure 5.1 XRD patterns of commercial ZrO_2 and CeO_2 catalysts.

32
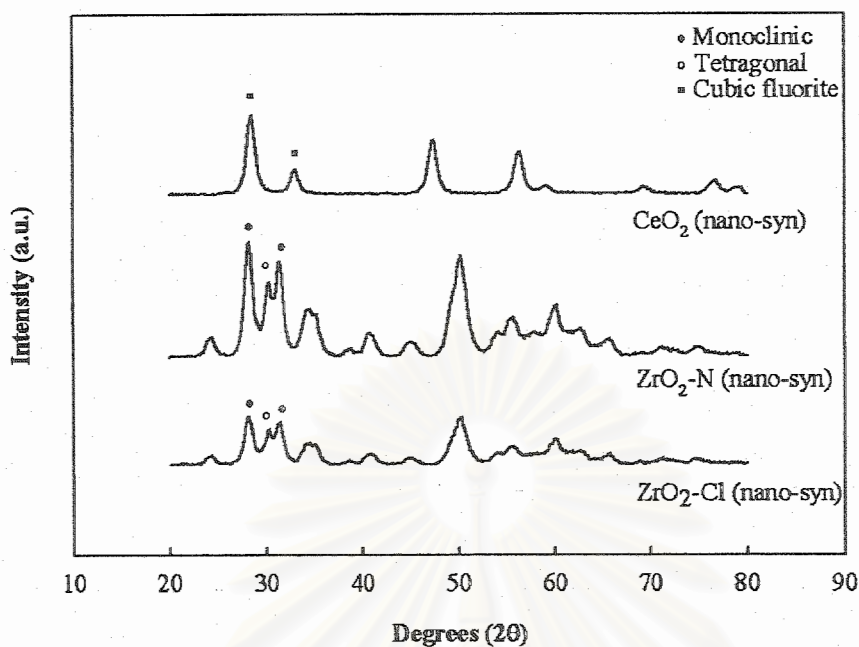
Figure 5.2 XRD patterns of synthesized ZrO_2 and CeO_2 catalysts.

Table 5.1 Summary of catalyst characteristics obtained from XRD measurement.

Catalysts	Phase	Average Crystal Size (nm)	Crystal Size (nm)[a]			% monoclinic phase[a]
			M[b]	T[c]	C[d]	
ZrO_2 (micron-com)	M	65.8	65.8	-	-	100
ZrO_2 (nano-com)	M, T	26.2	30.3	22.2	-	30
ZrO_2-Cl (nano-syn)	M, T	12.3	10.9	13.6	-	77
ZrO_2-N (nano-syn)	M, T	9.0	9.8	8.3	-	71
CeO_2 (micron-com)	C	135.9	-	-	135.9	-
CeO_2 (nano-syn)	C	8.1	-	-	8.1	-

[a] Based on XRD line broadening

[b] Monoclinic phase in ZrO_2

[c] Tetragonal phase in ZrO_2

[d] Cubic fluorite phase in CeO_2

33

5.1.1.2 N$_2$ Physisorption

The other physical properties of catalysts such as BET surface area, cumulative pore volume and average pore diameter were determined using the Micromeritics ASAP 2020 surface area and porosity analyzer. The values are summarized in **Table 5.2**. The micron- and nanoscale catalysts exhibited corresponding values based on their average crystallite sizes and BET surface areas. Compared to the micronscale catalysts, the nanoscale ones had smaller crystallite sizes which influenced not only on the increase in the cumulative pore volume, but also on the reduction of the average pore diameter. For the ZrO$_2$ prepared by different zirconium salt precursors, the resulted crystal structure was probably changed (Srinivasan and Davis, 1992). Su *et al.* (2000) and Wu and Yu (1990) found that SO$_4^{2-}$ from zirconium salt precursor such as Zr(SO$_4$)$_2$ affected crystallization and phase transformation of ZrO$_2$. The ZrO$_2$ prepared from Zr(SO$_4$)$_2$ showed both tetragonal phase and amorphous, but the ZrO$_2$ prepared from other zirconium salt precursors such as Zr(NO$_3$)$_4$, ZrCl$_4$ and ZrOCl$_2$ showed monoclinic and tetragonal phase. In this case, ZrO$_2$-Cl (nano-syn) and ZrO$_2$-N (nano-syn) were prepared from ZrOCl$_2$ and ZrO(NO$_3$)$_2$ as zirconium salt precursors, respectively. It was found that different precursors slightly affected the crystal structure in the phase composition of monoclinic/tetragonal phase over ZrO$_2$ and the BET surface area as well.

Table 5.2 N_2 Physisorption results.

Catalysts	BET Surface Area[a] (m^2/g)	Cumulative Pore Volume[b] (cm^3/g)	Average Pore Diameter[c] (nm)
ZrO_2 (micron-com)	6	0.012	9.5
ZrO_2 (nano-com)	41	0.115	9.9
ZrO_2-Cl (nano-syn)	95	0.173	4.8
ZrO_2-N (nano-syn)	92	0.169	4.9
CeO_2 (micron-com)	4	0.008	16.6
CeO_2 (nano-syn)	91	0.149	4.7

[a] Error of measurement $= \pm 5\%$.

[b] BJH desorption cumulative volume of pores between 1.7 and 300 nm diameter.

[c] BJH desorption average pore diameter.

5.1.1.3 Temperature programmed desorption (TPD)

The acid-base properties of the catalysts were measured by NH_3- and CO_2-TPD, respectively. The NH_3- and CO_2-TPD profiles are shown in **Figures 5.3** and **5.4**. From the TPD profiles, the amounts of acid and base sites which are also listed in **Table 5.3** were calculated from the area below curve. The characteristic peaks of these profiles are assigned to their desorption temperatures indicating the strength of Lewis surface sites. From NH_3-TPD results of Ma *et al.* (2005), it showed that NH_3 desorption peaks located at ca. 200°C and 300°C for ZrO_2 catalysts were corresponding to weak acid sites and moderate acid sites, respectively. Moreover, both peaks of monoclinic ZrO_2 exhibited slightly higher amount of acid sites compared to the tetragonal ZrO_2. In this work, all ZrO_2 mainly contained weak acid sites whereas the moderate acid sites were evident for the ZrO_2-N (nano-syn). This was probably due to more fraction of monoclinic phase present. The CeO_2 catalysts exhibited slightly different NH_3-TPD profiles from those of ZrO_2 catalysts.

Based on CO_2 desorption peaks, the weak base sites, moderate base sites and strong base sites can be identified (Ma *et al.*, 2005). It indicated that all kinds of base

35

sites were presented in the tetragonal ZrO_2 whereas only weak and moderate base sites were observed on the monoclinic ZrO_2. For CO_2-TPD profiles of ZrO_2 (**Figure 5.4**), the ZrO_2 (nano-com) exhibited higher desorption temperature than the other ZrO_2 catalysts due to more tetragonal phase in ZrO_2. Furthermore, the ZrO_2 (nano-com) had the highest amount of base sites among the other ZrO_2 catalysts indicating higher basicity of tetragonal ZrO_2 than monoclinic ZrO_2. For the CeO_2 catalysts, it contained only the weak base sites and moderate base sites. As a matter of fact, the ZrO_2 catalysts exhibited higher basicity than the CeO_2 catalysts. It should be mentioned that there were only a few acid and base sites for the micronscale catalysts (both ZrO_2 and CeO_2) compared to the nanoscale ones. It was suggested that differences in both acid and base sites can be attributed to the various fractions of crystal phases along with the crystallite sizes of catalysts. However, due to the presence of only one crystal phase in the ceria catalysts, the various acid and base sites present would be independent of crystal phase. Hence, different acid and base sites for ceria must be attributed to differences in crystallite sizes only. In fact, crystallite size also relates to BET surface area. Therefore, the amount of acid and base sites may be ascribed to effect of surface area. However, the two crystal phases of zirconia can be altered and consequently affected the acid-base properties. In order to give a better understanding, the relationship between acid-base sites and percent of tetragonal phase in ZrO_2 is illustrated in **Figure 5.5**. It was found that the amount of acid sites increased with increased percents of tetragonal phase in ZrO_2 up to a maximum at ca. 29%, and then decreased with more tetragonal phase present. In other words, there was an optimum point at 29% of the tetragonal phase in ZrO_2, which can maximize the acid sites. Considering the base sites, the amount of base sites was apparently proportional to the percent of tetragonal phase in ZrO_2. As a result, basicity increased with increasing of tetragonal phase in ZrO_2.
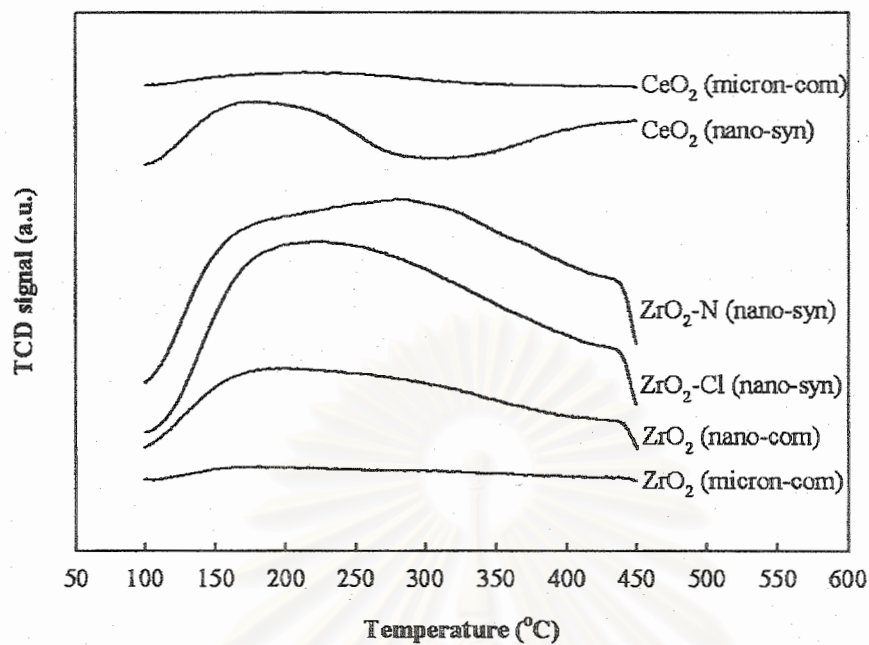
Figure 5.3 NH₃-TPD profiles of ZrO₂ and CeO₂ catalysts.
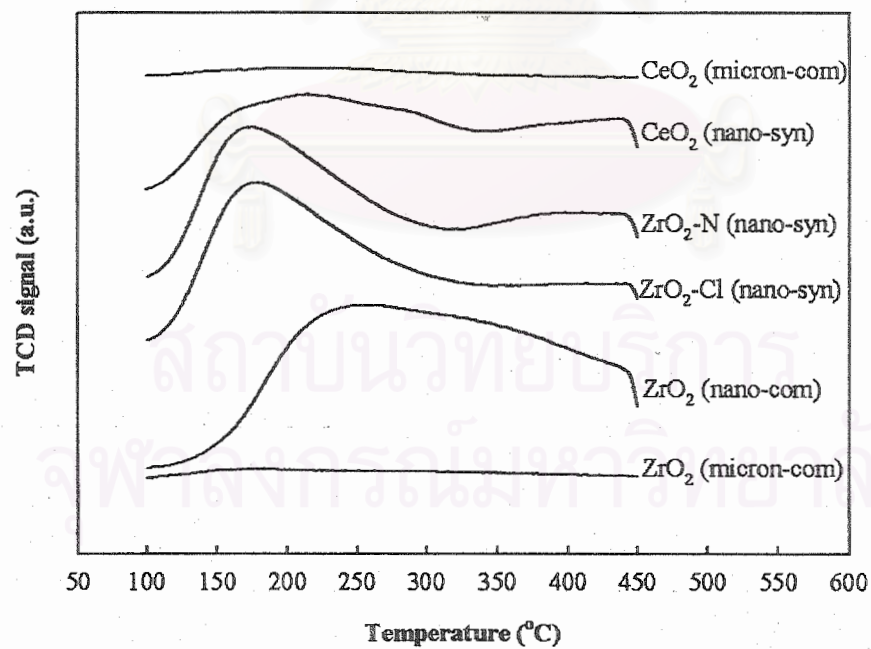
Figure 5.4 CO₂-TPD profiles of ZrO₂ and CeO₂ catalysts.

Table 5.3 Results from NH_3- and CO_2-TPD measurements.

Catalysts	Total Sites (μmole/g)	
	Acid Sites[a]	Base Sites[b]
ZrO_2 (micron-com)	24	15
ZrO_2 (nano-com)	160	319
ZrO_2-Cl (nano-syn)	361	191
ZrO_2-N (nano-syn)	389	188
CeO_2 (micron-com)	16	9
CeO_2 (nano-syn)	190	161

[a] From NH_3-TPD.

[b] From CO_2-TPD.
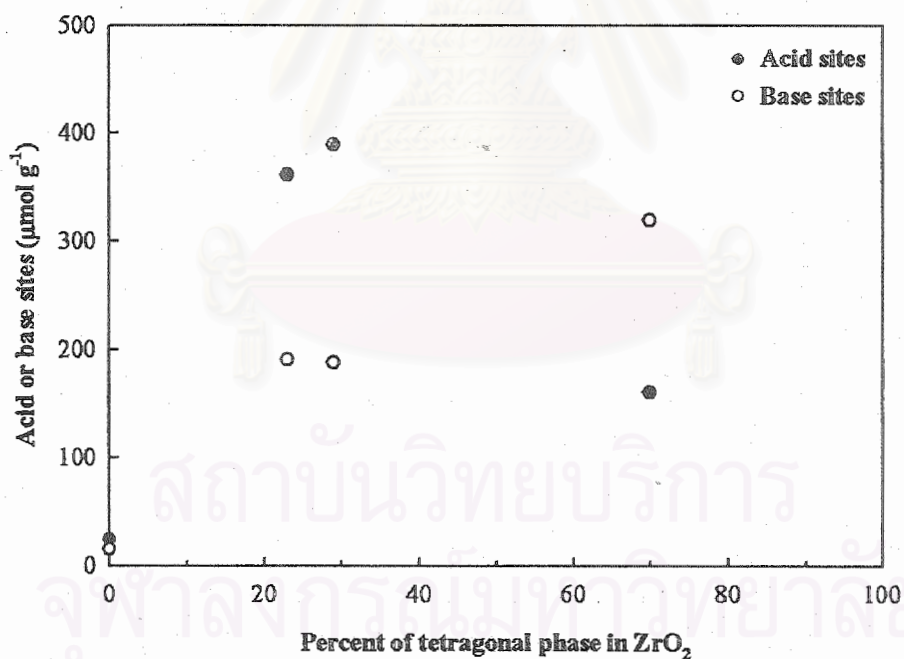
Figure 5.5 Relationship between amount of acid sites and base sites and percent of tetragonal in ZrO_2.

5.1.2 Catalytic Performance of isosynthesis over micron- and nanoscale ZrO₂ and CeO₂ catalysts

The commercial ZrO_2 and CeO_2 catalysts and synthesized ones were tested for their isosynthesis activity and selectivity at $400^{\circ}C$, atmospheric pressure and CO/H_2 of 1. A plot of reaction rates (based on products formed) versus the time-on-stream for all catalysts is shown in **Figure 5.6**. Typically, time-on-stream behavior for CO hydrogenation exhibits the highest activity at initial time and gradually decreases with more reaction times until the reaction reaches the steady-state rate indicating a constant activity. Therefore, activity profiles for isosynthesis were similar to typical activity profiles of CO hydrogenation. The steady-state rate was reached after 20 h and calculated as shown in **Table 5.4** along with the product selectivity in **Table 5.5**. It was found that the catalytic activities of the commercial microscale ZrO_2 and CeO_2 were low without any selectivity of isobutene in hydrocarbons. No significant differences were observed regarding their physical properties. The acid-base sites for both microscale catalysts were similar, but somehow, much fewer than those of the nanoscale ones. Therefore, the key factor that influenced the catalytic performance of the microscale ZrO_2 and CeO_2 was essentially the amount of acid-base sites of these catalysts. From the previous work (Su *et al.*, 2000, Li *et al.*, 2001, Li *et al.*, 2002, Li *et al.*, 2004), it was reported that the catalytic activity and selectivity of isobutene in hydrocarbons depended on the amount of acid and base sites of catalysts. The experimental results also revealed that the microscale ZrO_2 was selective for C_3 in hydrocarbons, but the microscale CeO_2 was selective for C_1 in hydrocarbons.

The synthesized nanoscale CeO_2 exhibited higher catalytic activity and selectivity for isobutene in hydrocarbons than the commercial microscale one. It was found that the nanoscale CeO_2 had much higher BET surface area and the amount of acid-base sites compared to the commercial microscale one. Even though, the crystallite sizes of CeO_2 changed, the crystal phase of them was identical. Hence, it was suggested that the increase in BET surface area and/or the acid-base properties probably rendered the nanoscale CeO_2 catalyst high catalytic performance. The tendencies of catalytic activity and selectivity of isobutene in hydrocarbons over the commercial micron- and nanoscale ZrO_2 were similar to those of CeO_2 according to the sizes. It was reported (Pichler and Ziesecke, 1949, Su *et al.*, 2000, Maruya *et al.*,

2000) that zirconia was the most selective catalyst in the isosynthesis and more effective than ceria (Pichler and Ziesecke, 1949), although it was also a selective catalyst for the formation of branched chain compounds such as isobutene in C_4 from syngas. Considering the commercial and synthesized nanoscale ZrO_2, the activity of the former exhibited less activity than the latter, but they had slightly difference in selectivity of isobutene in hydrocarbons (ca. 77-86%). The higher activity of the synthesized ZrO_2 could be due to higher amount of acid sites. The base property might slightly affect the reaction selectivity to isobutene; however, it was obscured by the higher activity. In this study, physical properties of the synthesized ZrO_2 with different zirconium salt precursor such as ZrO_2-Cl (nano-syn) and ZrO_2-N (nano-syn) did not change significantly. It was found that the ZrO_2-Cl (nano-syn) showed lower activity than the ZrO_2-N (nano-syn), which was possibly caused by lower amount of acid sites and a poison of Cl⁻. The result of selectivity to isobutene decreased because of higher activity. Considering the catalytic performance reported by early researchers (Su *et al.*, 2000), the ZrO_2-Cl (nano-syn) showed higher activity, but lower selectivity of isobutene in hydrocarbons than the ZrO_2-N (nano-syn). It was probably due to different conditions of ZrO_2 preparation such as the precipitated pH.

It should be noted that the highest catalytic activity of ZrO_2 appeared at the highest amount of acid sites. Considering the base properties, the amount of base sites largely increased when the crystallite size was decreased from micron- to nano-sized, and then resulted in higher selectivity of isobutene in hydrocarbons. However, the nanoscale ZrO_2 at different amounts of base sites did not significantly change the selectivity of isobutene. Moreover, it was found that there was higher activity for the nanoscale CeO_2 compared to the nanoscale ZrO_2. This tendency was also similar to the case of the micronscale ZrO_2 and CeO_2 catalysts. The physical properties of both nanoscale catalysts were similar whereas the amount of acid and base sites of ZrO_2 was higher than that of CeO_2. However, the catalytic performance was changed to the opposite trend, which was perhaps due to the difference in crystal phase between ZrO_2 and CeO_2.

According to the relationship between acid-base properties and percent of tetragonal phase in ZrO_2 (**Figure 5.5**), there was a maximum point at 29% tetragonal phase in ZrO_2 giving the highest amount of acid sites. It was the same trend as the relationship of the reaction rate and percent of tetragonal phase as shown in **Figure**

5.7. It can be concluded that the catalytic activity apparently associated with acidity. Considering the relationship between selectivity of isobutene in hydrocarbons and tetragonal phase, it was proposed that the selectivity of isobutene increased with the increase of the percent of tetragonal phase in ZrO_2, although it slightly changed when tetragonal phase appeared. In other words, the presence of tetragonal phase in zirconia rendered the better catalytic performance.

In addition, it was reported that when compared the high reaction pressure system to the low reaction pressure system, typically the latter exhibited lower catalytic activity, but higher selectivity of isobutene. Furthermore, lower reaction pressure may result in more selectivity of olefins, which was the same result as the previous work (Maruya *et al.*, 2000), than higher pressure system (Su *et al.*, 2000, Li *et al.*, 2001, Li *et al.*, 2002, Li *et al.*, 2003, Li *et al.*, 2004).

Table 5.4 Catalytic activity results from isosynthesis.

Catalysts	CO conversion (%)	Reaction rate (μmol kg cat^{-1} s^{-1})
ZrO_2 (micron-com)	0.19	6.3
ZrO_2 (nano-com)	1.21	40.7
ZrO_2-Cl (nano-syn)	1.47	49.3
ZrO_2-N (nano-syn)	2.90	97.3
CeO_2 (micron-com)	1.02	34.3
CeO_2 (nano-syn)	4.07	136.4

Table 5.5 Product selectivity results from isosynthesis.

Catalysts	Product selectivity in hydrocarbons[a] (mol%)			
	C_1	C_2	C_3	$i\text{-}C_4H_8$
ZrO_2 (micron-com)	11.8	10.8 (88.4)	77.4 (100.0)	0.0
ZrO_2 (nano-com)	5.6	2.7 (59.0)	9.5 (91.6)	82.2
ZrO_2-Cl (nano-syn)	2.7	2.6 (72.6)	9.2 (96.3)	85.5
ZrO_2-N (nano-syn)	6.0	5.6 (60.4)	11.1 (87.9)	77.3
CeO_2 (micron-com)	69.2	8.8 (43.7)	22.0 (93.3)	0.0
CeO_2 (nano-syn)	9.4	14.4 (58.4)	18.6 (65.2)	57.6

[a] Parentheses are the selectivity of olefin.
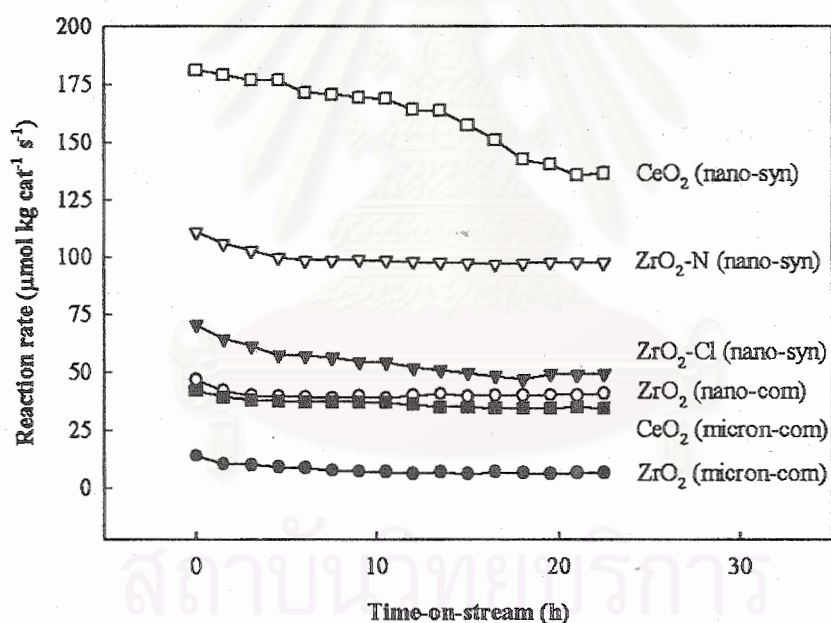

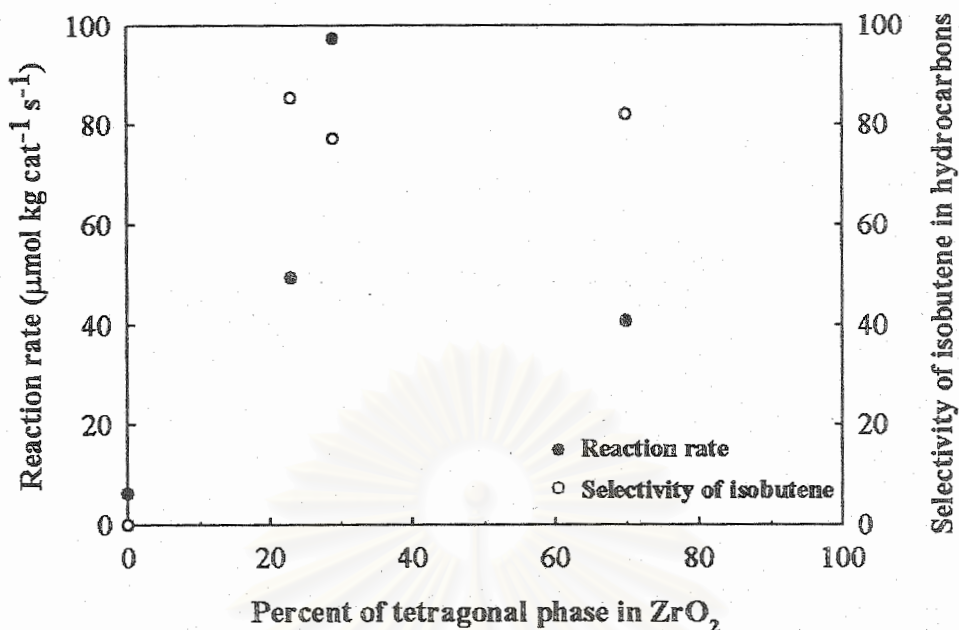**Figure 5.6** Time-on-stream behavior of ZrO_2 and CeO_2 catalysts.

Figure 5.7 Relationship between reaction rate and selectivity of isobutene in hydrocarbons and percent of tetragonal phase in ZrO_2.

5.2 Effect of temperature ramp during calcination on characteristics of nano-ZrO_2

To study the effect of temperature ramp during calcination, ZrO_2-N (nano-syn) from Section 5.1 was used in the study. Zirconia catalysts prepared by using temperature ramps of 1.0, 2.5, 5.0, 7.5 and 10.0°C/min were denoted as ZrO_2 (1.0), ZrO_2 (2.5), ZrO_2 (5.0), ZrO_2 (7.5) and ZrO_2 (10.0), respectively.

5.2.1 Catalyst Characterization

5.2.1.1 X-ray Diffraction (XRD)

Considering the preparation condition of ZrO_2 catalysts, the varied temperature ramps during calcination resulted in changes in both crystallite size and crystal phase. The XRD spectra of those ZrO_2 catalysts are illustrated in **Figure 5.8**. Based on calculation from XRD spectra, the average crystallite size of those catalysts are also listed in **Table 5.6** indicating the values ranging between 7 and 12 nm.

Considering the characteristic peak areas of monoclinic and tetragonal phases (**Figure 5.8**), it was observed that the latter was more dominant than the former upon increased temperature ramp during calcination. In addition, the phase composition of each ZrO_2 catalyst can be calculated as shown in **Table 5.6**. The results showed that the fraction of tetragonal phase increased with increased temperature ramp during calcination. According to monoclinic-tetragonal phase transformation of zirconia, the tetragonal phase should be formed above $1170^{\circ}C$, but the zirconia prepared by precipitation from aqueous salt solution can be occurred as a metastable tetragonal phase at low temperature. Moreover, the transformation of the matastable tetragonal form into the monoclinic form was probably due to the lower surface energy of the tetragonal phase compared to monoclinic phase (Tani, *et al.*, 1982, Osendi *et al.*, 1985). In fact, phase transformation of catalyst can be occurred by varying not only the calcination temperature, but also the heating rate of calcination being employed. In this case, lower temperature ramp would result in better heat distribution over surface and longer contact times. Thus, this may contribute to higher stabilized crystal phase of ZrO_2, leading to more monoclinic phase present.
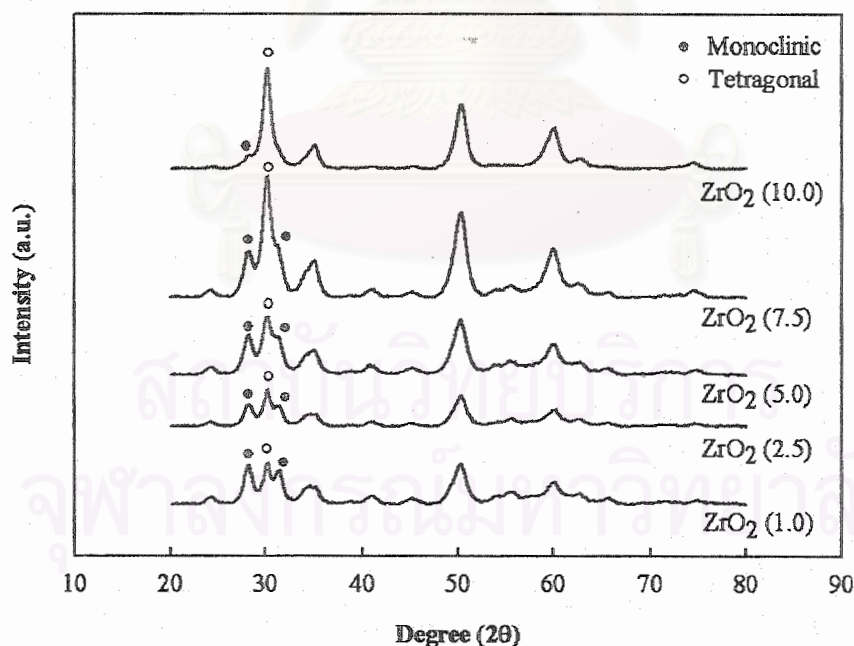

Figure 5.8 XRD patterns of different ZrO_2 catalysts with various temperature ramps during calcination.

Table 5.6 Characteristics of ZrO_2 with various temperature ramps during calcination.

Catalysts	Phase	Average Crystal Size (nm)	Crystal Size (nm)[a]		% tetragonal phase[a]
			M^b	T^c	
ZrO_2 (1.0)	M, T	9.0	9.8	8.3	29
ZrO_2 (2.5)	M, T	11.3	11.4	11.3	46
ZrO_2 (5.0)	M, T	8.6	8.7	8.6	43
ZrO_2 (7.5)	M, T	7.5	7.5	7.5	55
ZrO_2 (10.0)	M, T	7.8	6.5	9.0	85

[a] Based on XRD line broadening.

[b] Monoclinic phase in ZrO_2.

[c] Tetragonal phase in ZrO_2.

5.2.1.2 N_2 Physisorption

The physical properties of ZrO_2 catalysts characterized by means of N_2 physisorption such as BET surface area, cumulative pore volume and average pore diameter are summarized in **Table 5.7**. These ZrO_2 catalysts had specific surface areas ranging between ca. 92-106 m^2/g. For cumulative pore volume and average pore diameter, no differences were observed in all ZrO_2 catalysts, except for the ZrO_2 (10.0) where the decrease in both properties was evident. This was probably due to sintering of catalysts when high temperature ramp during calcination was applied. Therefore, it can be concluded that the temperature ramp during calcination did not significantly affect the surface areas of samples.

Table 5.7 N_2 Physisorption results.

Catalysts	BET Surface Area[a] (m^2/g)	Cumulative Pore Volume[b] (cm^3/g)	Average Pore Diameter[c] (nm)
ZrO_2 (1.0)	92	0.169	4.9
ZrO_2 (2.5)	100	0.172	4.7
ZrO_2 (5.0)	103	0.199	5.4
ZrO_2 (7.5)	106	0.191	5.0
ZrO_2 (10.0)	100	0.139	3.7

[a] Error of measurement = ±5%.

[b] BJH desorption cumulative volume of pores between 1.7 and 300 nm diameter.

[c] BJH desorption average pore diameter.

5.2.1.3 Temperature programmed desorption (TPD)

NH_3- and CO_2-TPD profiles of ZrO_2 catalysts with various temperature ramps during calcination are shown in **Figures 5.9** and **5.10**, respectively. All NH_3-TPD profiles in **Figure 5.9** exhibited the similar desorption profiles consisting mainly weak acid sites. Moreover, the amount of acid sites was in the range of ca. 387-428 μmole/g as listed in **Table 5.8** indicating not much difference. Considering the acidity of these catalysts, it slightly increased with increasing the fraction of tetragonal phase in ZrO_2. This tendency was also observed for the relationship between basicity and percent of tetragonal phase in ZrO_2 as illustrated in **Figure 5.11**. For CO_2-TPD profiles (**Figure 5.10**), the CO_2 desorption peaks at low temperature appeared in all profiles. It was suggested that all ZrO_2 catalysts had weak base sites. However, the increase in temperature ramp during calcination resulted in higher desorption temperature and areas under its curve as well. As mentioned in **Section 5.1.1.3**, the presence of more tetragonal in ZrO_2 was attributed to higher basicity of catalysts, especially for moderate and strong base sites. Therefore, the highest basicity of the ZrO_2 (10.0) was due to the highest tetragonal phase in ZrO_2.
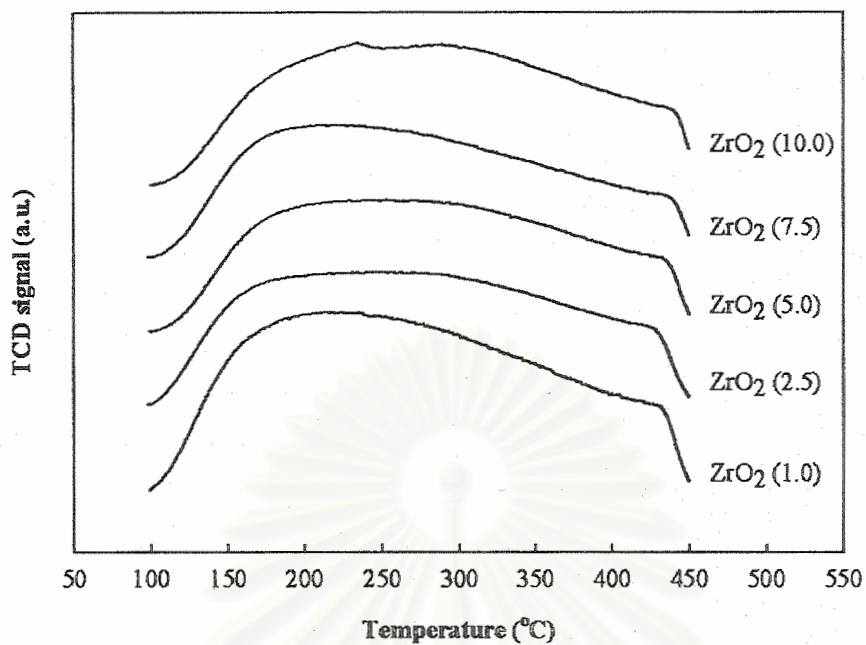
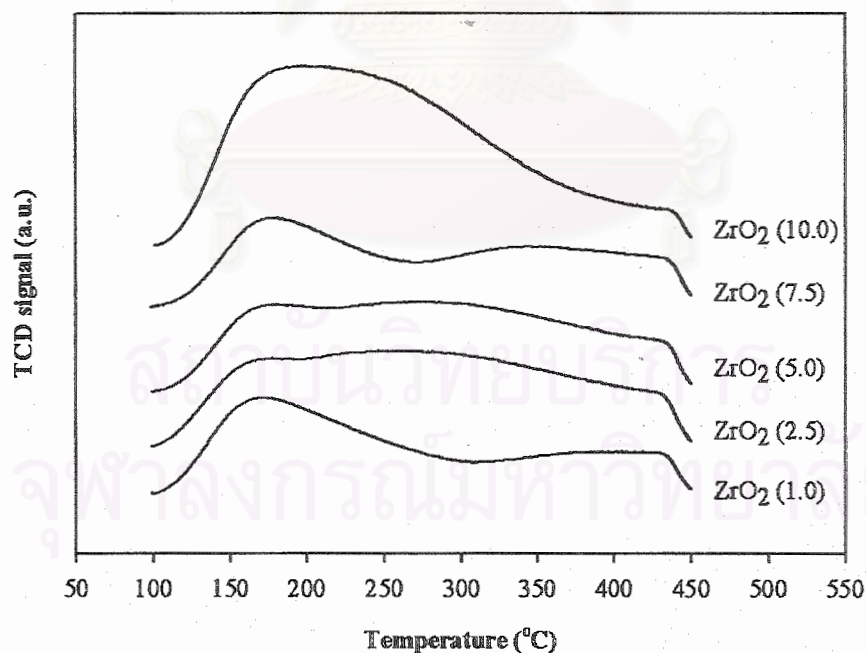**Figure 5.9** NH$_3$-TPD profiles of different ZrO$_2$ catalysts in various temperature ramps during calcination.

Figure 5.10 CO$_2$-TPD profiles of different ZrO$_2$ catalysts in various temperature ramps during calcination.

47

Table 5.8 Results from NH_3- and CO_2-TPD.

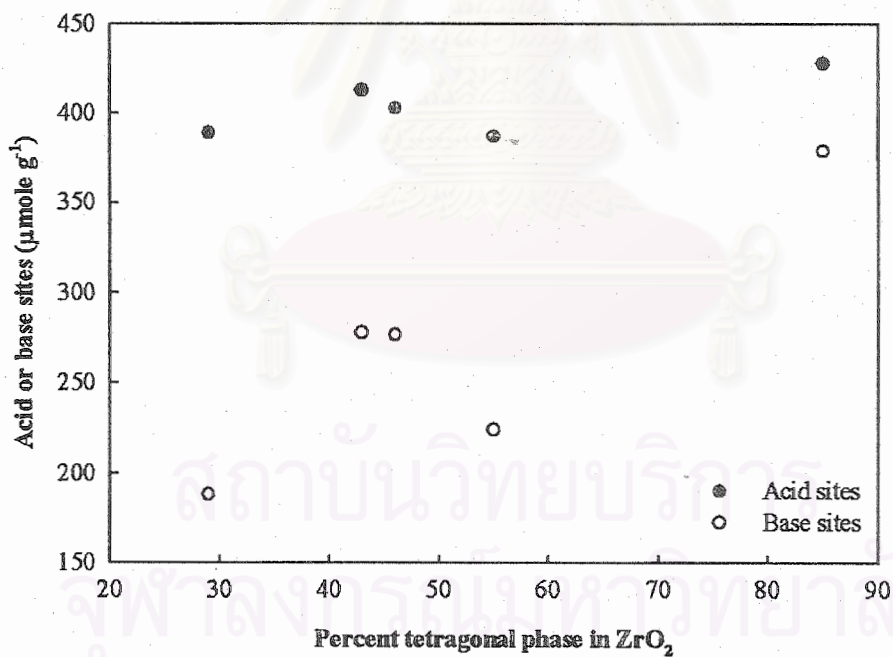| Catalysts	Total Sites ($\mu mole/g$)	
	Acid Sites[a]	Base Sites[b]
ZrO_2 (1.0)	389	188
ZrO_2 (2.5)	403	277
ZrO_2 (5.0)	413	278
ZrO_2 (7.5)	387	224
ZrO_2 (10.0)	428	379

[a] From NH_3-TPD.

[b] From CO_2-TPD.

Figure 5.11 Relationship between amount of acid sites and base sites and percent of tetragonal in ZrO_2.

5.2.1.4 Electron spin resonance spectroscopy (ESR)

A spin of unpaired electron was detected by means of ESR to identify defect center of zirconia considerably assumed as the existence of Zr^{3+} sites. Zr^{3+} signals represented at $g_\perp \sim 1.97$ and $g_\parallel \sim 1.95$ as shown the example in **Figure 5.12** were very close to the positions of Zr^{3+} on ZrO_2 surface observed by many researchers as reported in **Table 5.9**. Only $g_\perp$ was considered in this work due to the apparent signal. The relative ESR intensity at various ZrO_2 is shown in **Figure 5.13**. It was found that quantity of Zr^{3+} varied with various the temperature ramps during calcination. The result showed that Zr^{3+} gradually increased with increased heating rate of calcination up to the highest intensity at ca. 5°C/min, and then rapidly decreased beyond that value. From the early researches (Zhao et al., 2004, Anpo et al., 1990), it reasonably suggested that the Zr^{3+} center to ESR can be described as the oxygen coordinatively unsaturated zirconium sites on ZrO_2 surface. In addition, they proposed the removal of the surface hydroxyl account for the formation of the new Zr^{3+} sites. It was possibly due to the presence of hydroxyl groups combined in a position of coordinatively unsaturated sites resulting in less Zr^{3+} intensity. Therefore, changing of Zr^{3+} intensity in this case may be attributed to loss of the surface O atoms, especially hydroxyl groups, on ZrO_2 surface. Low heating rate of calcination can remove hydroxyl group more than high heating rate because the former had a long times for releasing hydroxyl group compared to the latter. As seen at calcined temperature ramp at 7.5 and 10°C/min, it obviously showed a decreased relative intensity of Zr^{3+}. Moreover, it was also found the relationship between tetragonal phase in ZrO_2 and Zr^{3+} intensity as illustrated in **Figure 5.14**. It showed the highest intensity of Zr^{3+} at ca. 43% of tetragonal phase in ZrO_2, then decreased almost linearly upon increased tetragonal phase in ZrO_2.
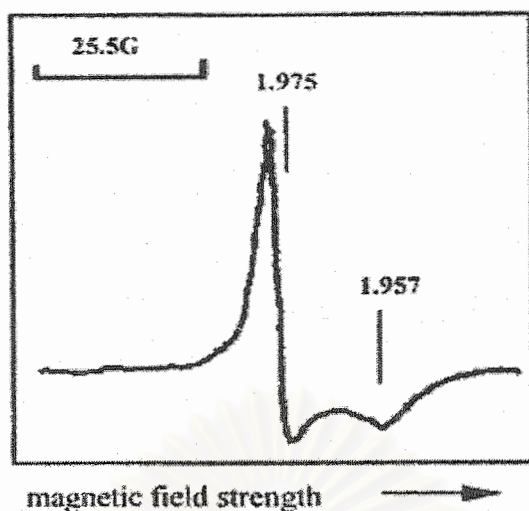
25.5G

1.975

1.957

magnetic field strength

Figure 5.12 ESR spectrum of ZrO_2 (Zhao *et al.*, 2004).

Table 5.9 ESR parameters of Zr^{3+} observed from different references.

| Paramagnetic ion	g-value	Reference
Zr^{3+} in ZrO_2	$g_\parallel = 1.956$	Torralvo and Alario, 1984
	$g_\perp = 1.981$	
Zr^{3+} in ZrO_2	$g_\parallel = 1.953$	Moterra *et al.*, 1990
	$g_\perp = 1.978$	
Zr^{3+} in sulfated zirconia	$g_\parallel = 1.951$	Chen *et al.*, 1993
	$g_\perp = 1.979$	
Zr^{3+} in ZrO_2	$g_\parallel = 1.961$	Liu *et al.*, 1995
	$g_\perp = 1.974$	
Zr^{3+} in V_2O_5/ZrO_2	$g_\perp = 1.97$	Adamski *et al.*, 1999
Zr^{3+} in sulfated zirconia	$g_\parallel = 1.967$	Carlos *et al.*, 1999
	$g_\perp = 1.982$	
Zr^{3+} in $Pt/WO_x/ZrO_2$	$g_\parallel = 1.96$	Punnoose and Seehra, 2002
	$g_\perp = 1.98$	
Zr^{3+} in ZrO_2	$g_\parallel = 1.957$	Zhao *et al.*, 2004
	$g_\perp = 1.975$	
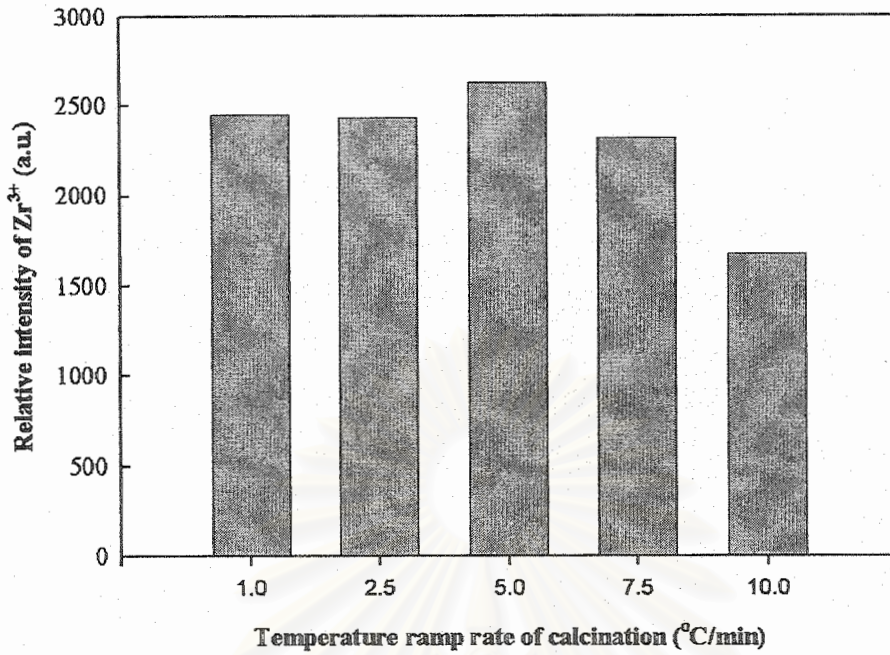
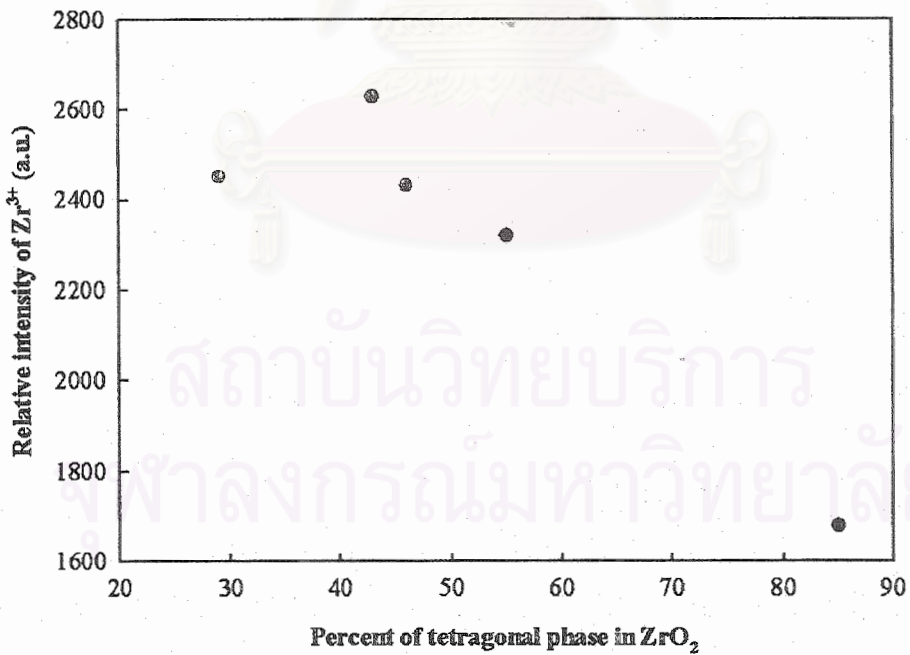**Figure 5.13** Relative ESR intensity of various ZrO_2 catalysts.

Figure 5.14 Relationship between percent of tetragonal phase in ZrO_2 and quantity of Zr^{3+}.

5.2.2 Catalytic performance of isosynthesis over ZrO_2 catalysts with various temperature ramps during calcination

For various temperature ramps during calcination, it showed the catalytic performance of various ZrO_2 catalysts at these conditions as listed in **Tables 5.10** and **5.11**. To describe the behavior of product selectivity of isobutene, the amount of Zr^{3+} was a major factor affecting its performance, which was shown in **Figure 5.15**. It was obvious that the ZrO_2 (5.0) exhibited the highest intensity of Zr^{3+}, corresponding to the highest selectivity of isobutene in hydrocarbons. Considering the results with temperature ramps during calcination of 2.5, 5.0 and 7.5°C/min, it can be concluded that the relative intensity of Zr^{3+} was related to the heating rate of calcination. Although ZrO_2 (5.0) and ZrO_2 (7.5) performed the highest product selectivity of isobutene, both catalysts had different Zr^{3+} intensity. The ZrO_2 (7.5) had lower quantity of Zr^{3+} than the ZrO_2 (5.0). Both catalysts would have another factor affecting the selectivity of isobutene in hydrocarbons, which may be attributed to the presence of tetragonal phase in ZrO_2. Increase in tetragonal phase in ZrO_2 probably resulted in higher selectivity of isobutene in hydrocarbons. Therefore, increase in tetragonal phase in ZrO_2 (7.5) affected the high selectivity of isobutene in hydrocarbons even at low content of Zr^{3+}. Comparison of ZrO_2 (7.5) and ZrO_2 (10.0) performances, it can be observed that the effect of Zr^{3+} intensity was more effective than that of tetragonal phase. As a result, the latter exhibited lower selectivity of isobutene in hydrocarbons. As known, the presence of tetragonal phase in ZrO_2 apparently related to the amount of acid and base sites as mentioned in **Section 5.2.1.3**. Therefore, it revealed that there were many factors affecting the product selectivity of isobutene. However, the intensity of Zr^{3+} and tetragonal phase in ZrO_2 were dominant factors. Based on the results of Li et al. (1997), it revealed that there was a close linear relation between Zr^{3+} ion and the selectivity to isobutene for reaction over ZrO_2. Those results showed that Zr^{3+} ion might involve in CO hydrogenation. This possibly proposed the mechanism of the catalytic reaction via a surface species $Zr(III)(CO)_2$. Considering the activity, the amount of acid sites did not relate to the activity. The activity was disproportional to the product selectivity of isobutene in hydrocarbons. From **Table 5.10**, it reported that ZrO_2 (2.5) exhibited the highest activity among all ZrO_2 catalysts.

Table 5.10 The catalytic activity results from isosynthesis.

Catalysts	CO conversion (%)	Reaction rate (μmol kg cat^{-1} s^{-1})
ZrO_2 (1.0)	2.90	97.3
ZrO_2 (2.5)	3.97	133.0
ZrO_2 (5.0)	1.91	63.9
ZrO_2 (7.5)	1.82	61.0
ZrO_2 (10.0)	3.15	105.5

Table 5.11 Product selectivity results from isosynthesis.

Catalysts	Product selectivity in hydrocarbons[a] (mol%)			
	C_1	C_2	C_3	i-C_4H_8
ZrO_2 (1.0)	6.0	5.6 (60.4)	11.1 (87.9)	77.3
ZrO_2 (2.5)	7.6	9.0 (62.8)	14.2 (85.5)	69.2
ZrO_2 (5.0)	3.8	3.8 (65.1)	9.5 (93.5)	82.9
ZrO_2 (7.5)	3.8	3.7 (66.9)	9.5 (94.0)	82.9
ZrO_2 (10.0)	7.7	7.3 (60.2)	11.5 (86.1)	73.4

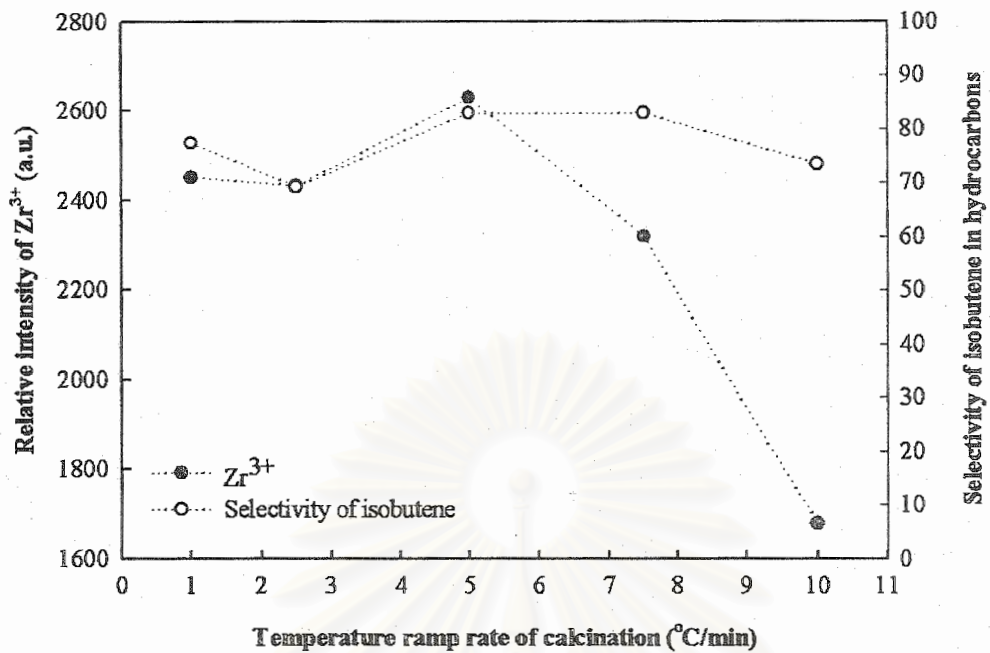[a] Parentheses are the selectivity of olefin.

Figure 5.15 Relationship between temperature ramp during calcination and intensity of Zr^{3+} along with selectivity of isobutene in hydrocarbons.

CHAPTER VI

CONCLUSIONS AND RECOMMENDATION

6.1 Conclusions

The conclusions of the present research are the following:

1. The nanoscale zirconia and ceria exhibited higher catalytic activity and selecitivity of isobutene in hydrocarbons than micronscale ones did. Besides the acid-base properties obtained from CO_2 and NH_3-TPD analysis, the fraction of tetragonal phase in zirconia apparently affected the catalytic properties.

2. The difference in temperature ramp during calcination of zirconia catalysts can be altered the phase composition in zirconia coupled with the intensity of Zr^{3+} obtained from ESR measurement. The product selectivity of isobutene depended on both quantities of Zr^{3+} and tetragonal fraction in zirconia catalyst whereas the acid site did not significant change upon various temperature ramp during calcination process.

6.2 Recommendation for future study

From the previous conclusions, the following recommendations for the future study are proposed as follows:

1. Investigation for the use of mixed oxides of ZrO_2-CeO_2 on the isosynthesis should be further performed.
2. Effect of reaction temperatures on the catalytic performance should be further investigated as well.
3. Catalyst modification should be considered to find a better catalyst.

REFERENCES

Adamski, A., Sojka, Z., Dyrek, Z., and Che, M. An XRD and ESR study of V_2O_5/ZrO_2 catalysts: influence of the phase transitions of ZrO_2 on the migration of V^{4+} ions into zirconia. *Solid State Ionics.* 177 (1999): 113-122.

Anpo, M., and Nomura, T. Photoluminescence and FT-IR studies of the dissociative adsorption of H-2 on the active ZrO_2 catalyst and its role in the hydrogenation of CO. *Res. Chem. Intermed.* 13 (1990): 195-202.

Bamwenda, R. and Arakawa, H. Cerium dioxide as a photocatalyst for water decomposition to O_2 in the presence of Ce^{4+}_{aq} and Fe^{3+}_{aq} species. *J. Mol. Catal. A: Chem.* 161 (2000): 105-113.

Carlos, R.V., Carlos, L.P., Kiyoyuki, S., Carlos, A., and Jose, M.P. Coking of SO_4^{2-}-ZrO_2 catalysts during isomerization of n-butane and its relation to the reaction mechanism. *J. Catal.* 187 (1999): 39-49.

Chen, F.R., Coudurier, G., Joly, J.R., and Vedrine, J.C. Superacid and catalytic properties of sulfated zirconia. *J. Catal.* 143 (1993): 616-626.

Cormack, A.N., and Parker, S.C., Some Observations on the Role of Dopants in Phase Transitions in Zirconia from Atomistic Simulations. *J. Am . Ceram. Soc.* 73 (1990): 3220-3224.

Courty, P.,and Marcilly, C.Scientific approach to the preparation of bulk mixed oxide catalysts. *Stud. Surf. Sci. Catal.* 16 (1983): 485-519.

Ekerdt, J.G., and Jackson, N.B. The surface characteristics required for isosynthesis over zirconium dioxide and modified zirconium dioxide. *J. Catal.* 126 (1990): 31-45.

Ekerdt, J.G., and Jackson, N.B. Isotope studies of the effect of acid sites on the reactions of C_3 intermediates during isosynthesis over zirconium dioxide and modified zirconium dioxide. *J. Catal.* 126 (1990): 46-56.

Ekerdt, J.G., Tseng, S.C., and Jackson, N.B. Isosynthesis reactions of CO/H_2 over zirconium dioxide. *J. Catal.* 109 (1988): 284-297.

Ertl, G., Knozinger, H., and Weitkamp, J. *Handbook of Heterogeneous Catalysis Volume 1.* Weinheim: VCH, 1997.

Farrauto, R. J., and Bartholomew, C. H. *Fundamentals of Industrial Catalytic Processes.* 1 st ed. London: Chapman & Hall, 1997.

Garvie, R. C. Stabilization of the tetragonal structure in zirconia microcrystals. *J. Phys. Chem.* 82 (1978): 218-224.

Heuer, A. H. Transformation Toughening in ZrO_2-containing Ceramics. *J. Am. Ceram. Soc.* 70 (1987): 689-698.

Li, Y.W., He, D.H., Cheng, Z.X., Su, C.L., Li, J.R., and Zhu, Q.M. Effect of calcium salts on isosynthesis over ZrO_2 catalysts. *J. Mol. Catal. A: Chem.* 175 (2001): 267-275.

Li, Y.W., He, D.H., Yuan, Y.B., Cheng, Z.X., and Zhu, Q.M. Influence of acidic and basic properties of ZrO_2 based catalysts on isosynthesis. *Fuel.* 81 (2002): 1611-1617.

Li, Y.W., He, D.H., Zhang, Q.J., Xu, B.Q., and Zhu, Q.M. Influence of reactor materials on i-C_4 synthesis from CO hydrogenation over ZrO_2 based catalysts. *Fuel. Process. Tech.* 83 (2003): 39-48.

Li, Y.W., He, D.H., Zhu, Q.M., Zhang, X., and Xu, B.Q. Effects of redox properties and acid-base properties on isosynthesis over ZrO_2-based catalysts. *J. Catal.* 221 (2004): 584-593.

Liu, H., Zhang, X., and Xue, Q. ESR Characterization of ZrO_2 nanopowder. *J. Phys. Chem.* 99 (1995): 332-334.

Livage, J., Doi, K., and Mazieres, C. Nature and thermal evolution of amorphous hydrated zirconium oxide. *J. Am. Ceram. Soc.* 51 (1968): 349-353.

Ma, Z.-Y., Yang, C., Wei, W., Li, W.-H., and Sun, Y.-H. Surface properties and CO adsorption on zirconia polymorohs. *J. Mol. Catal. A: Chem.* 227 (2005): 119-124.

Maruya, K., Ito, K., Kushihashi, K., Kishida, Y., Domen, K., and Onishi, T. Isoprene formation from CO and H_2 over CeO_2 catalysts. *Catal. Lett.* 14 (1992): 123-126.

Maruya, K., Kawamura, M., Aikawa, M., Hara, M., and Arai, T. Reaction path of methoxy species to isobutene and its dependence on oxide catalysts in CO hydrogenation. *J. Organ. Chem.* 551 (1998): 101-105.

Maruya, K., Komiya, T., Hayakawa, T., Lu, L., and Yashima, M. Active sites on ZrO_2 for the formation of isobutene from CO and H_2. *J. Mol. Catal. A: Chem.* 159 (2000): 97-102.

Maruya, K., Takasawa, A., Haraoka, T., Domen, K., and Onishi, T. Role of methoxide species in isobutene formation from CO and H_2 over oxide catalysts

Methoxide species in isobutene formation. *J. Mol. Catal. A: Chem.* 112 (1996):143-151.

Mercera, P.D.L., van Ommen, J.G., Doesburg, E.B.M., Burggraaf, and Ross, J.R.H. Zirconia as a support for catalysts. Influence of additives on the thermal stability of the porous texture of monoclinic zirconia. *Appl. Catal.* 71 (1991): 363-391.

Morterra, C., Giamello, E., Orio, L., and Volante, M. Formation and reactivity of Zr^{3+} centers at the surface of vacuum-activated monoclinic zirconia. *J. Phys. Chem.* 94 (1990): 3111-3116.

Osendi, M. I., Moya, J. S., Sena, C. J., and Soria, J. Metastability of tetragonal zirconia powder. *J. Am. Ceram. Soc.* 68 (1985): 135-139.

Peshev, P., Toshev, A., and Gyurov, G. Preparation of high-dispersity MCo_2O_4 (M=Mg, Ni, Zn) spinels by thermal dissociation of coprecipitated oxalates. *Mater. Res. Bull.* 24 (1989): 33-40.

Pichler, H. Twenty five years of synthesis of gasoline by catalytic conversion of carbon monoxide and hydrogen. *Adv. Catal.* 4 (1952): 271-341.

Pichler, H., and Ziesecke, K.H. Some properties of solid paraffins produced from carbon monoxide and hydrogen at high pressures. *Brennst. Chem.* 30 (1949): 1-13.

Punnoose, A., and Seehra, M.S. ESR observation of W^{5+} and Zr^{3+} states in $Pt/WO_x/ZrO_2$ catalysts. *Catal. Lett.* 78 (2002): 157-160.

Sato, T., Katakura, T., Yin, S., Fujimoto,T., and Yabe, S. Synthesis and UV-shielding properties of calcia-doped ceria nanoparticles coated with amorphous silica. *Solid State Ionics.* 172 (2004): 377-382.

Sofianos, A. Production of branched-chain hydrocarbons via isosynthesis. *Catal. Today.* 15 (1992): 149-175.

Srinivasan, R., and Davis, B.H. Influence of zirconium salt precursors on the crystal-structures of zirconia. *Catal. Lett.* 14 (1992): 165.

Srinivasan, R., De Angelis, R. J., Ice, G., and Davis, B. H. Critical Particle-Size and Phase-Transformation in Zirconia-Transformation Electron-Microscopy and X-Ray-Diffraction Studies. *J. Am. Ceram. Soc.* 73 (1990): 3528-3530.

Stiles, A.B. *Laboratory and Commercial Preparations.* New York: Marcel Dekker, 1983.

Su, C.L., He, D.H., Li, J.R., Cheng, Z.X., and Zhu, Q.M. Influences of preparation parameters on the structural and catalytic performance of zirconia in isosynthesis. *J. Mol. Catal. A: Chem.* 153 (2000): 139-146.

Su, C.L., Li, J.R., He, D.H., Cheng, Z.X., and Zhu, Q.M. Synthesis of isobutene from synthesis gas over nanosize zirconia catalysts. *Appl. Catal. A: General* 202 (2000): 81-89.

Tani, E., Yoshimura, M., and Somiya, S. Formation of Ultrafine tetragonal ZrO_2 powder under hydrothermal conditions. *J. Am. Ceram. Soc.* 66 (1982): 11-14.

Thomas, C.L. *Catalytic Processes and Proven Catalysts.* New York: Academic Press, 1970.

Torralvo, M.J. and Alario, M.A. Crystallization behavior of zirconium oxide gels. *J. Catal.* 86 (1984): 473-476.

Wender, I. Reactions of synthesis gas. *Fuel Proc.* 48 (1996): 189-297.

West, A. R. *Solid State Chemistry and its Application,* Brisbane: John Wiley & Sons, 1997.

Wu, F.C., and Yu, S.C. Effects of H_2SO_4 on the crystallization and phase transformation of zirconia powder in the precipitation processes. *J. Mater. Sci.* 25 (1990): 970-976.

Zhao, Q., Wang, X., and Cai, T. The study of surface properties of ZrO2. *Appl. Surf. Sci.* 225 (2004): 7-13.

APPENDICES

APPENDIX A

CALCULATION OF CRYSTALLITE SIZE

Calculation of crystallite size by Debye-Scherrer equation

The crystallite size was calculated from the half-height width of the diffraction peak of XRD pattern using the Debye-Scherrer equation.

From Scherrer equation:

$$D = \frac{K\lambda}{\beta\cos\theta} \qquad (A.1)$$

where D = Crystallite size, Å

K = Crystallite-shape factor (= 0.9)

λ = X-ray wavelength (= 1.5418 Å for CuKα)

θ = Observed peak angle, degree

β = X-ray diffraction broadening, radian.

The X-ray diffraction broadening (β) is the pure width of powder diffraction free from all broadening due to the experimental equipment. α-Alumina is used as a standard sample to observe the instrumental broadening since its crystallite size is larger than 2000 Å. The X-ray diffraction broadening (β) can be obtained by using Warren's formula.

From Warren's formula:

$$\beta = \sqrt{B_M^2 - B_S^2} \qquad (A.2)$$

where B_M = the measured peak width in radians at half peak height

B_S = the corresponding width of the standard material.

Example: Calculation of the crystallite size of zirconia

The half-height width of 111_m diffraction peak = 0.25° (from Figure A.1)

$$= \left(\frac{2\pi}{360}\right) \cdot (0.25)$$

$$= 0.0044 \text{ radian}$$

The corresponding half-height width of peak of α-alumina (from the B_S value at the 2θ of 28.36° in Figure A.2) = 0.0039 radian

The pure width, β $\quad = \quad \sqrt{B_M^2 - B_S^2}$

$$= \quad \sqrt{0.0044^2 - 0.0039^2}$$

$$= \quad 0.0021 \text{ radian}$$

$\beta \quad = \quad 0.0021$ radian

$2\theta \quad = \quad 28.36°$

$\theta \quad = \quad 14.18°$

$\lambda \quad = \quad 1.5418 \text{ Å}$

The crystallite size $\quad = \quad \dfrac{0.9 \times 1.5418}{0.0021 \times \cos 14.18°}$

$$= \quad 678 \text{ Å}$$

$$= \quad 67.8 \text{ nm}$$
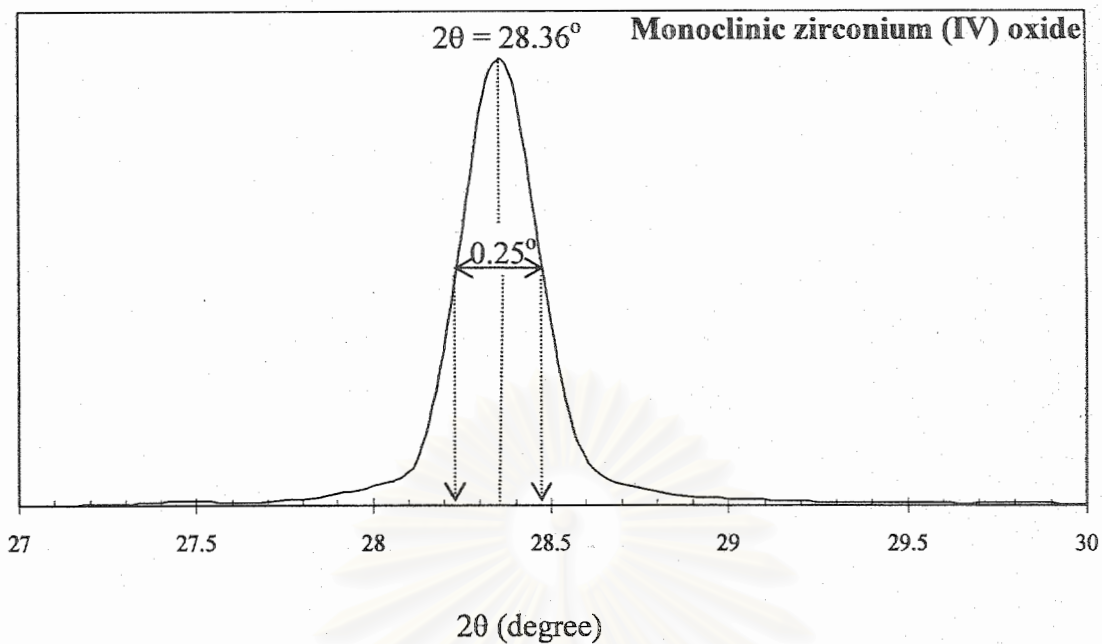
Figure A.1 The 111_m diffraction peak of zirconia for calculation of the crystallite size.
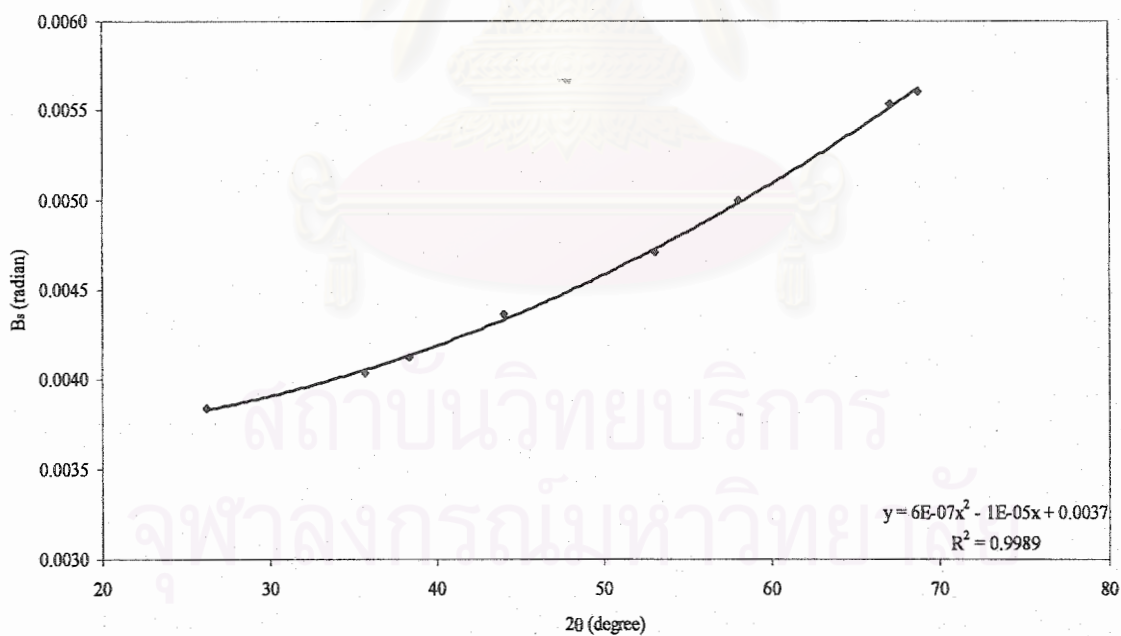
Figure A.2 The plot indicating the value of line broadening due to the equipment (data were obtained by using α-alumina as a standard).

APPENDIX B

CALCULATION OF FRACTION OF CRYSTAL PHASE
OF ZIRCONIA

The fraction of crystal phase of zirconia was estimated from X-ray diffraction (XRD) profile. The amounts of tetragonal and monoclinic phase present in the zirconia were estimated by comparing the areas of characteristic peaks of the monoclinic phase ($2\theta = 28$ and 31 for (111) and (111) reflexes, respectively) and the tetragonal phase ($2\theta = 30$ for the (111) reflex). The fraction composition of each phase was calculated from the Gaussian areas $h \times w$.

$$\text{Fraction of monoclinic phase} \quad = \quad \frac{\sum (h \times w) \text{ monoclinic phase}}{\sum (h \times w) \text{ monoclinic and tetragonal phase}} \quad \text{(B.1)}$$

$$\text{Fraction of tetragonal phase} \quad = \quad \frac{\sum (h \times w) \text{ tetragonal phase}}{\sum (h \times w) \text{ monoclinic and tetragonal phase}} \quad \text{(B.2)}$$

where h = the height of X-ray diffraction pattern at the characteristic peaks

w = the half-height width of X-ray diffraction pattern at the characteristic peaks.

Example: Calculation of the fraction of crystal phase of zirconia

Table B.1 Calculation of the fraction of crystal phase of zirconia

Crystal phase	2θ	h	w	$h \times w$	Fraction of crystal phase
Monoclinic	28.24	2577	0.29	747.33	
	31.56	1837	0.32	587.84	
	Total			1335.17	0.30
Tetragonal	30.28	8348	0.37	3088.76	0.70
Total				4423.93	1.00
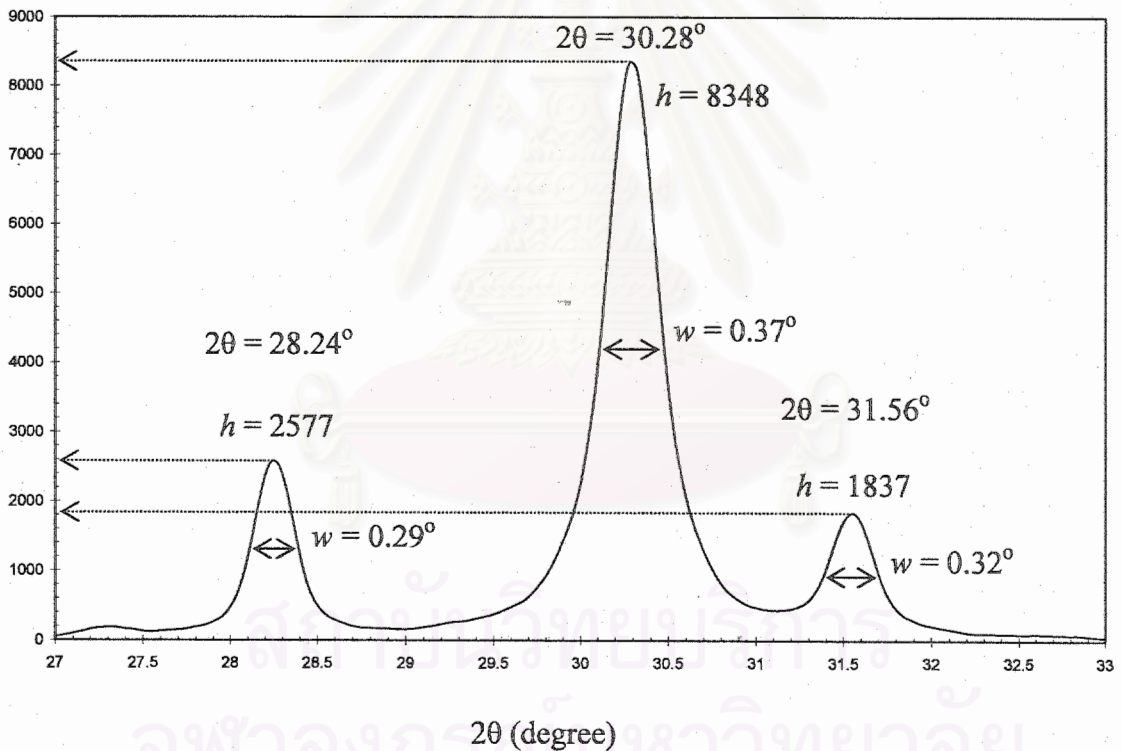
Figure B.1 The X-ray diffraction peaks of zirconia (nanopowder) for calculation of the fraction of crystal phase of zirconia.

APPENDIX C

CALIBRATION CURVES

This appendix showed the calibration curves for calculation of reactant and product compositions in isosynthesis. The reactants are carbon monoxide and hydrogen while the products are carbon dioxide and hydrocarbons consisting of C_1-C_4 such as methane, ethane, ethylene, propane, propylene, n-butane, isobutane, isobutene. For isosynthesis, the main product in hydrocarbons is isobutene.

The gas chromatography with a thermal conductivity detector (TCD), Shimadzu model 8A was used for analyzing the concentration of carbon monoxide and carbon dioxide by using Molecular sieve 5A column and Porapak-Q column, respectively.

The VZ-10 column was used in a gas chromatography equipped with a flame ionization detector (FID), Shimadzu model 14B, for analyzing the concentration of products including of methane, ethane, ethylene, propane, propylene, n-butane, isobutane, isobutene. Conditions used in both GCs are illustrated in Table B.1.

The calibration curves exhibit the relationship between mole of gas component (y-axis) and peak area reported from gas chromatography (x-axis). The calibration curves of carbon monoxide, carbon dioxide, methane, ethane, ethylene, propane, propylene, n-butane, isobutane and isobutene are shown in the following figures.

Table C.1 Conditions of Gas chromatograpy, Shimadzu model GC-8A and GC-14B.

Parameters	Condition	
	Shimadzu GC-8A	Shimadzu GC-14B
Width	5	5
Slope	50	50
Drift	0	0
Min. area	10	10
T.DBL	0	0
Stop time	30	90
Atten	5	0
Speed	2	2
Method	41	41
Format	1	1
SPL.WT	100	100
IS.WT	1	1

สถาบันวิทยบริการ
จุฬาลงกรณ์มหาวิทยาลัย
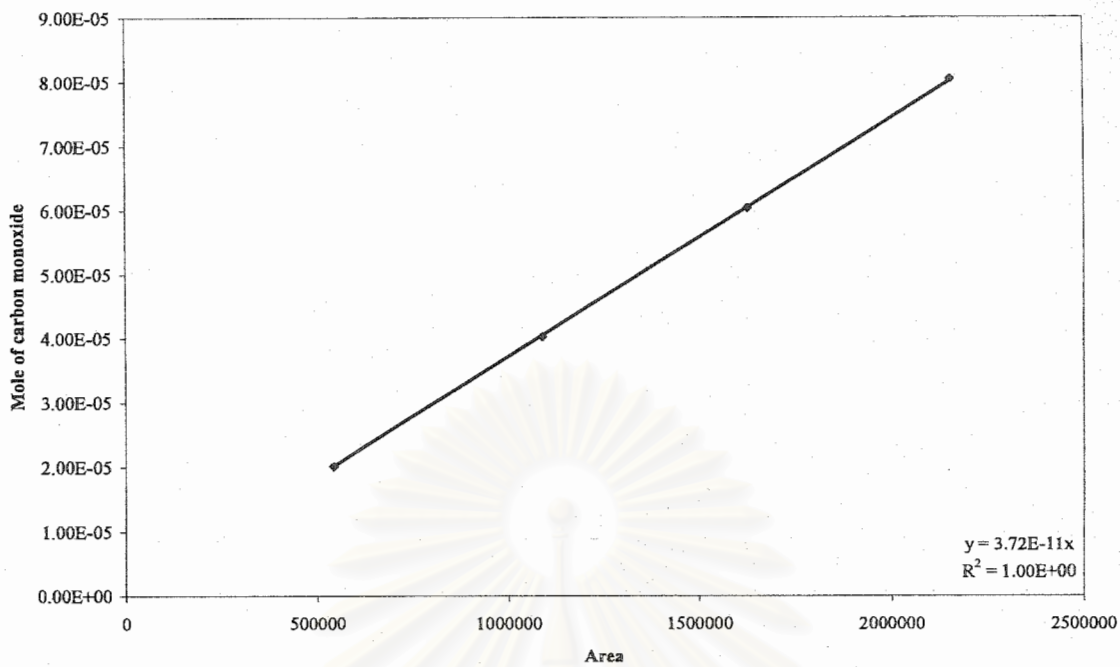
Figure C.1 The calibration curve of carbon monoxide.
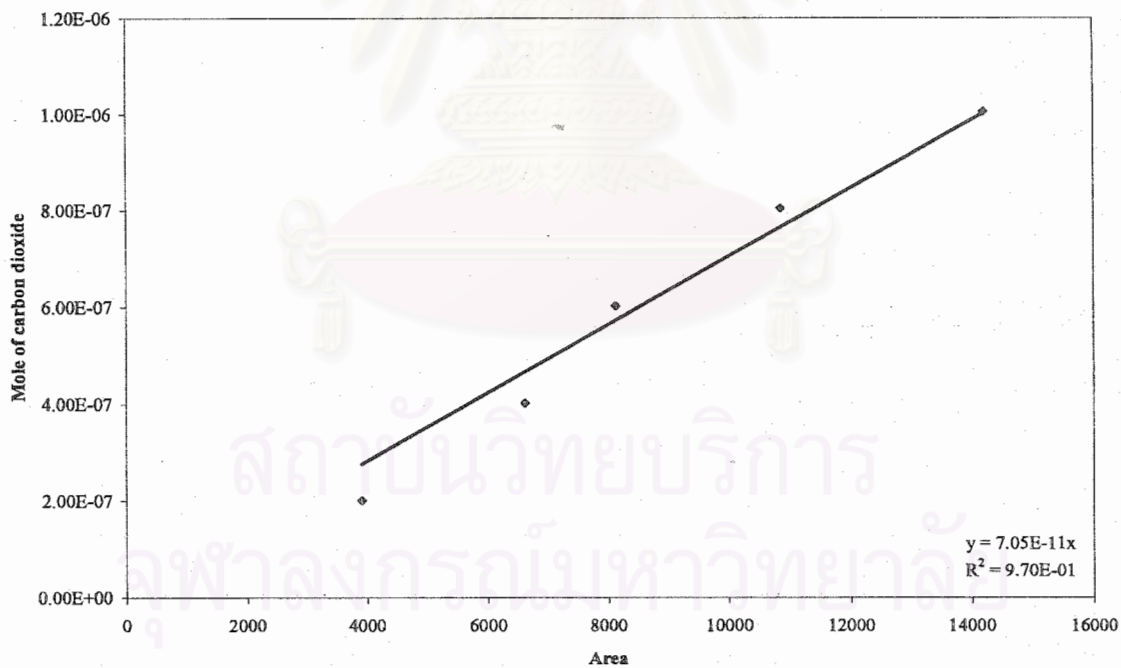
Figure C.2 The calibration curve of carbon dioxide.
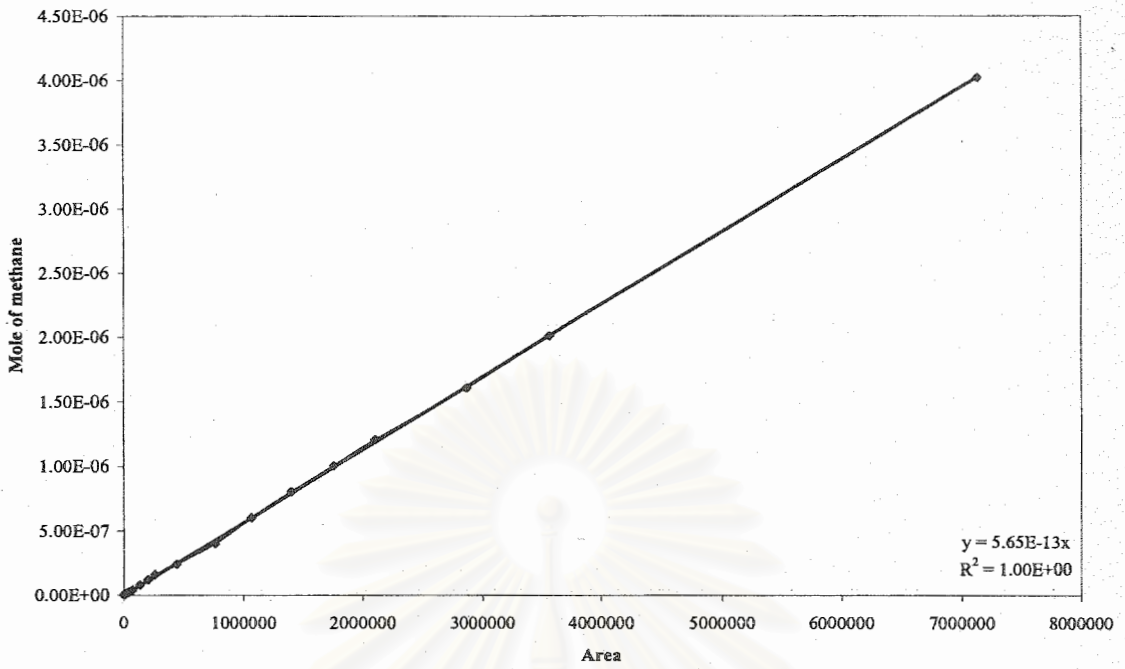
Figure C.3 The calibration curve of methane.
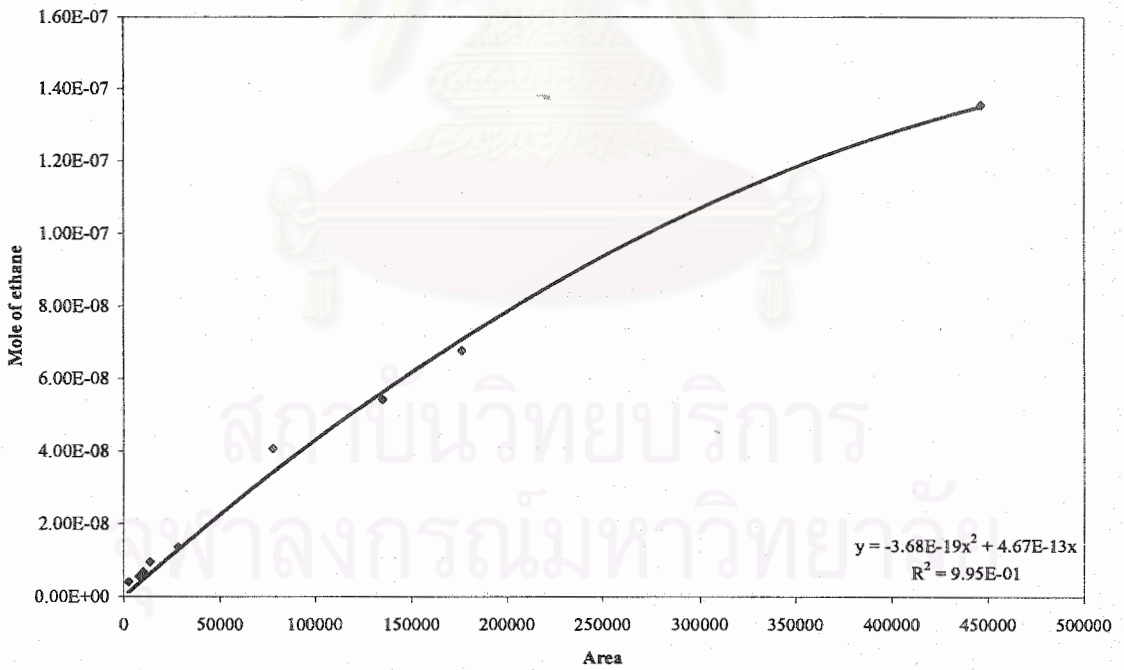
Figure C.4 The calibration curve of ethane.
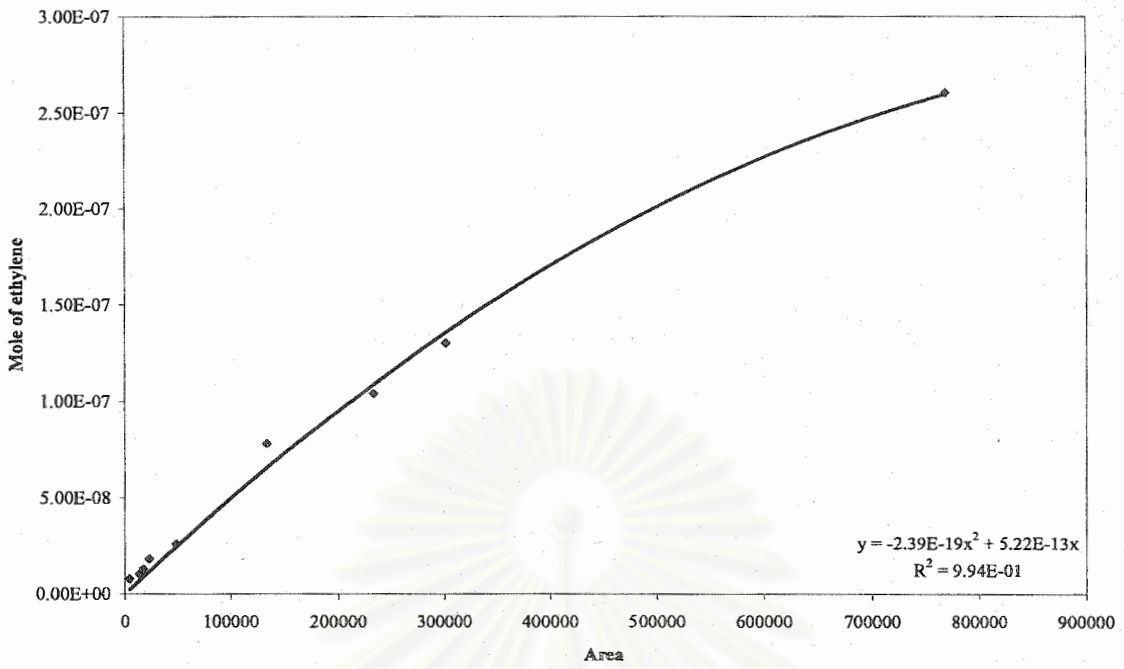
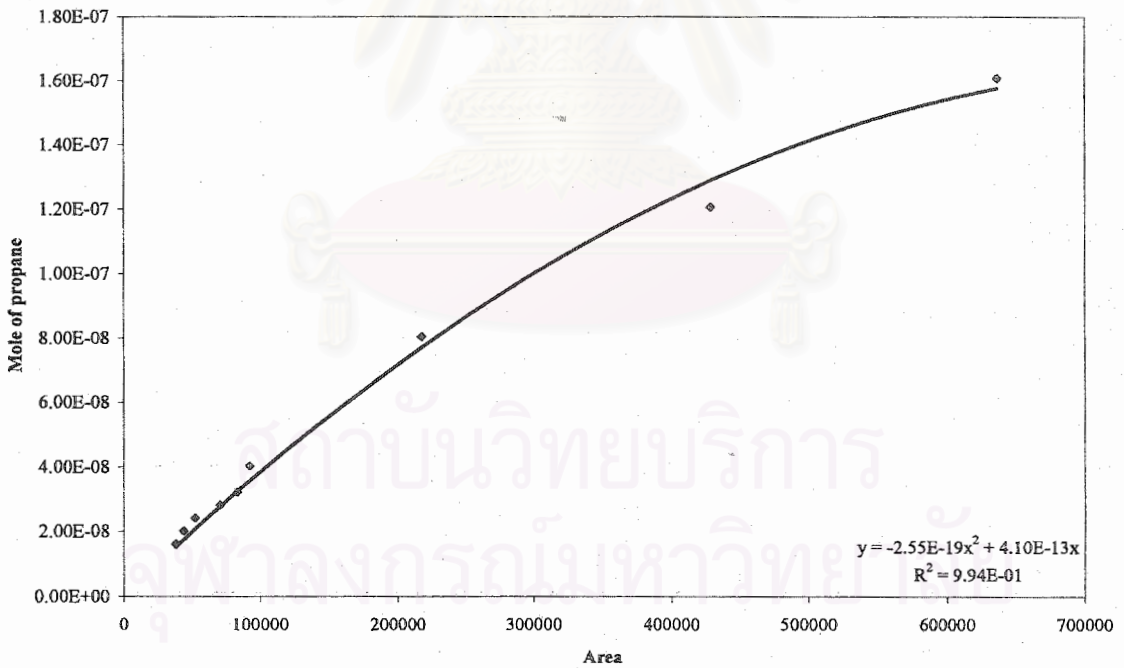**Figure C.5** The calibration curve of ethylene.

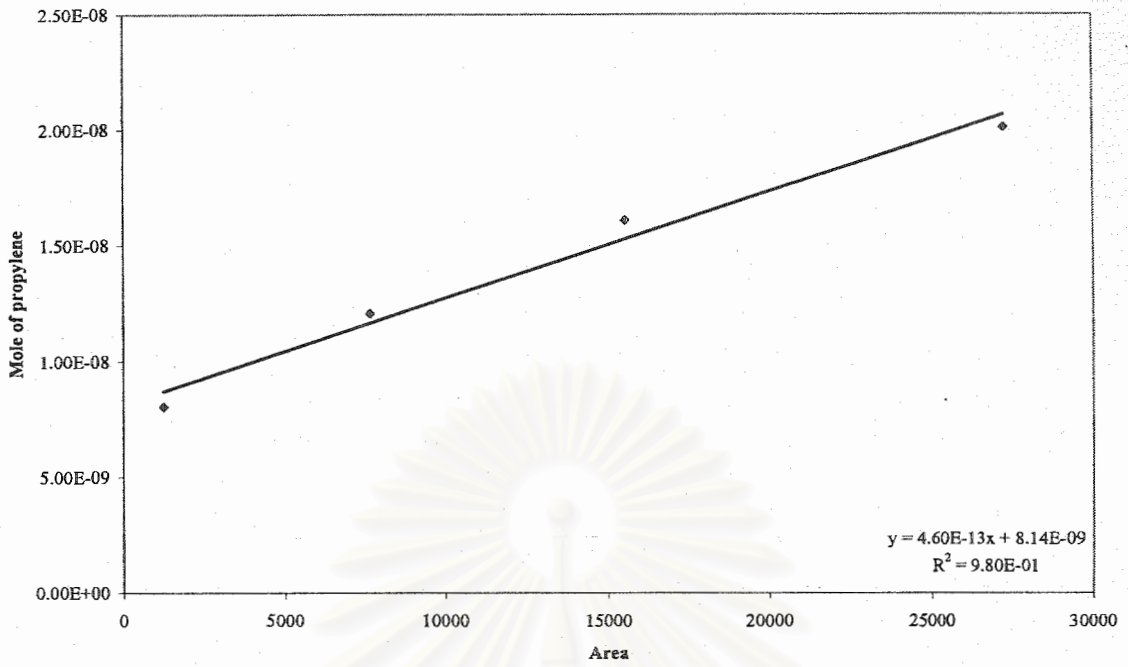**Figure C.6** The calibration curve of propane.

Figure C.7 The calibration curve of propylene.
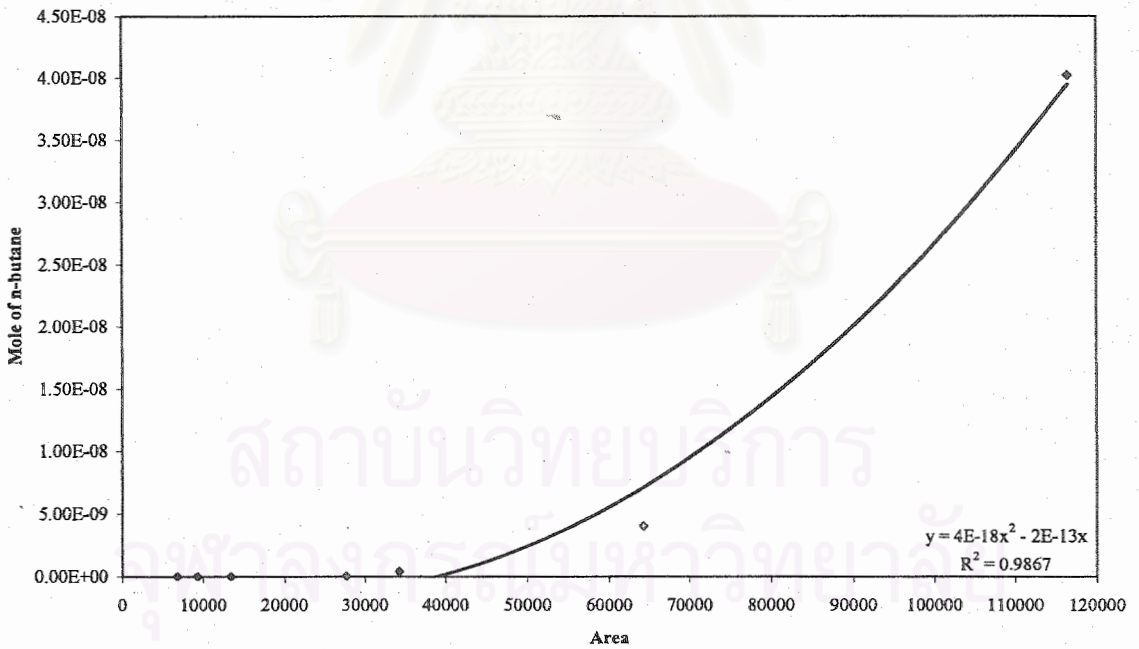

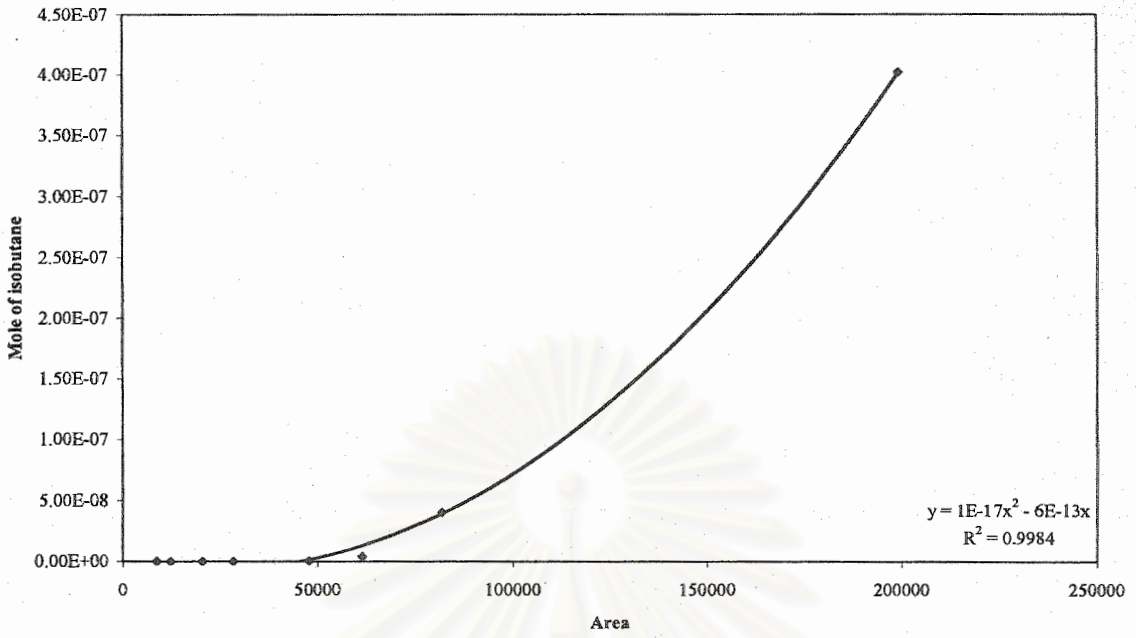**Figure C.8** The calibration curve of n-butane.

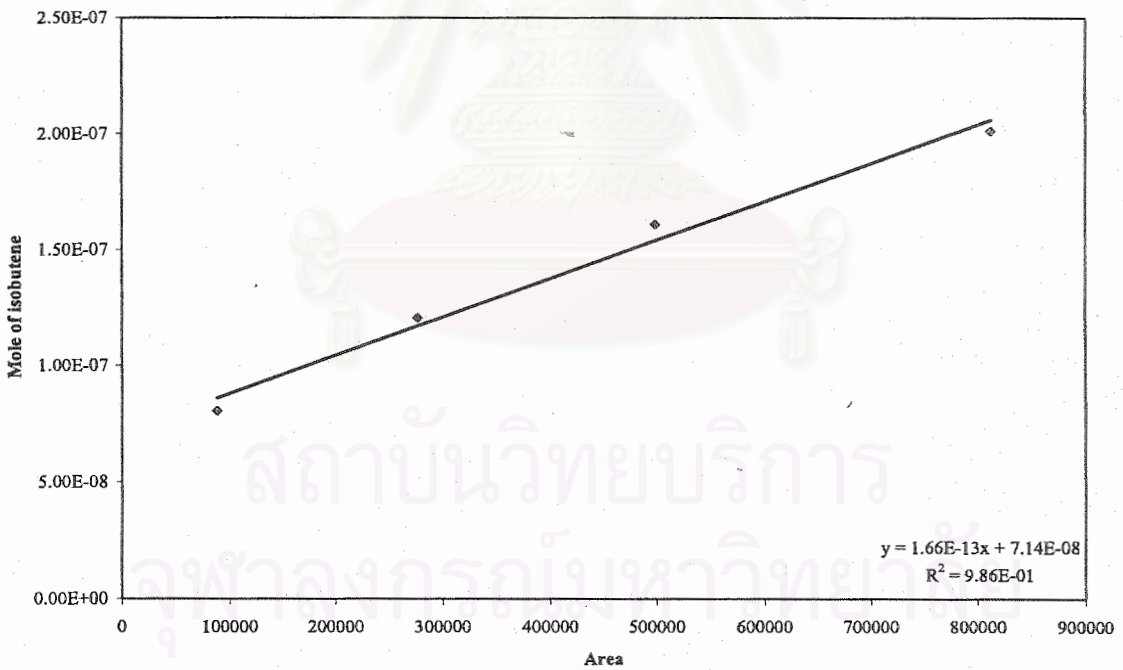**Figure C.9** The calibration curve of isobutane.

Figure C.10 The calibration curve of isobutene.

APPENDIX D

CALCULATIONS OF CARBON MONOXIDE CONVERSION, REACTION RATE AND SELECTIVITY

The catalytic performance for the isosynthesis was evaluated in terms of CO conversion, reaction rate and selectivity.

CO conversion is defined as moles of CO converted with respect to moles of CO in feed:

$$\text{CO conversion (\%)} = \frac{\text{moles of CO converted to product}}{\text{moles of CO in feed}} \times 100 \qquad \text{(D.1)}$$

where mole of CO can be determined from CO peak area of the product gas and the calibration curve of CO (Figure C.1 in Appendix C).

$$\text{Mole of CO} = (\text{Area of CO peak from integrator plot on GC-8A}) \times 3.72 \times 10^{-11}$$

$$\text{(D.2)}$$

Reaction rate was calculated from CO conversion as follows:

Let the weight of catalyst used	=	W	g
Flow rate of CO	=	10	cm^3/min
Volume of 1 mole of gas at STP	=	22400	cm^3
Temperature of gas at STP	=	273 K	
Room temperature of gas	=	303 K	

$$\text{Reaction rate (\mu mole/kg catalyst/s)} = \frac{[\%\text{conversion of CO}/100] \times 22400 \times 303 \times 10^6}{W \times 10 \times 60 \times 273}$$

$$\text{(D.3)}$$

Selectivity of product is defined as moles of carbon in the product of interest (B) with respect to moles of CO converted:

$$\text{Selectivity of B (\%)} = \frac{\text{moles of B formed}}{\text{moles of CO converted}} \times 100 \qquad \text{(D.4)}$$

where B is product, mole of B can be measured employing the calibration curves of products such as CO_2 and hydrocarbon C_1-C_4 such as methane, ethane, ethylene, propane, propylene, n-butane, isobutane and isobutene as shown in Figures C.2-C.10 of Appendix C.

$$\text{Mole of methane} = (\text{Area of methane peak from integrator plot on GC-14B}) \times 5.65 \times 10^{-13}$$
$$\text{(D.5)}$$